Field characterization of the PM$_{2.5}$ Aerosol Chemical Speciation Monitor: insights into the composition, sources and processes of fine particles in Eastern China

5   Yunjiang Zhang[1,2,3,4], Lili Tang[1,2], Philip L. Croteau[5], Olivier Favez[3], Yele Sun[6,7,8], Manjula R. Canagaratna[5], Zhuang Wang[1], Florian Couvidat[3], Alexandre Albinet[3], Hongliang Zhang[9], Jean Sciare[10], André S. H. Prévôt[11], John T. Jayne[5], Douglas R. Worsnop[5]

[1]Jiangsu Collaborative Innovation Center of Atmospheric Environment and Equipment Technology,

10   Nanjing University of Information Science and Technology, Nanjing 210044, China

[2]Jiangsu Environmental Monitoring Center, Nanjing 210036, China

[3]Institut National de l'Environnement Industriel et des Risques, Verneuil en Halatte, 60550, France

[4]Laboratoire des Sciences du Climat et de l'Environnement, CNRS-CEA-UVSQ, Université Paris-Saclay, Gif sur Yvette, 91191, France

15   [5]Aerodyne Research, Inc., Billerica, Massachusetts 01821, United States

[6]State Key Laboratory of Atmospheric Boundary Layer Physics and Atmospheric Chemistry, Institute of Atmospheric Physics, Chinese Academy of Sciences, Beijing 100029, China

[7]Center for Excellence in Regional Atmospheric Environment, Institute of Urban Environment, Chinese Academy of Sciences, Xiamen 361021, China

20   [8]University of Chinese Academy of Sciences, Beijing 100049, China

[9]Nanjing Handa Environmental Science and Technology Limited, Nanjing 211102, China

[10]The Cyprus Institute, Environment Energy and Water Research Center, Nicosia, Cyprus

[11]Laboratory of Atmospheric Chemistry, Paul Scherrer Institute, Villigen PSI 5232, Switzerland

25   Correspondence to: Lili Tang (lily3258@163.com) and Yele Sun (sunyele@mail.iap.ac.cn)

Abstract

A $PM_{2.5}$-capable aerosol chemical speciation monitor (Q-ACSM) was deployed in urban Nanjing, China for the first time to measure in-situ non-refractory fine particle (NR-$PM_{2.5}$) composition from October 20 to November 19, 2015 along with parallel measurements of submicron aerosol (PM_1) species by a standard Q-ACSM. Our results show that the NR-$PM_{2.5}$ species (organics, sulfate, nitrate, and ammonium) measured by the $PM_{2.5}$-Q-ACSM are highly correlated ($r^2 > 0.9$) with those measured by a Sunset Lab OC/EC Analyzer and a Monitor for AeRosols and GAses (MARGA). The comparisons between the two Q-ACSMs illustrated similar temporal variations in all NR species between PM_1 and $PM_{2.5}$, yet substantial mass fractions of aerosol species were observed in the size range of 1–2.5 µm. On average, NR-$PM_{1-2.5}$ contributed 53 % of the total NR-$PM_{2.5}$ with sulfate and secondary organic aerosols (SOA) being the two largest contributors (26 % and 27 %, respectively). Positive matrix factorization of organic aerosol showed similar temporal variations in both primary and secondary OA between PM_1 and $PM_{2.5}$ although the mass spectra were slightly different due to more thermal decomposition on the capture vaporizer of the $PM_{2.5}$-Q-ACSM. We observed an enhancement of SOA under high relative humidity conditions, which is associated with simultaneous increases in aerosol pH, gas-phase species (NO_2, SO_2, and NH_3) concentrations and aerosol water content driven by secondary inorganic aerosols. These results likely indicate an enhanced reactive uptake of SOA precursors upon aqueous particles. Therefore, reducing anthropogenic NO_x, SO_2, and NH_3 emissions might not only reduce secondary inorganic aerosols but also the SOA burden during haze episodes in China.

1 Introduction

Atmospheric fine particles (PM$_{2.5}$, aerodynamic diameter $\leqslant$ 2.5 µm) are of great concern because they degrade air quality (Zhang et al., 2015a), reduce visibility (Watson, 2002) and negatively affect human health (Pope and Dockery, 2006). PM$_{2.5}$ also has potential impacts upon global climate change and ecosystems. However, the impacts remain highly uncertain, mainly due to their complex chemical and microphysical properties, and sources (Huang et al., 2014; Sun et al., 2014), and the unclear interactions between meteorology and atmospheric aerosols (Sun et al., 2015; Ding et al., 2016). Therefore, continuous measurements of aerosol particle composition particularly in a complete level with high time-resolution (e.g., less than 1 hour) are essential to understand the variations and formation mechanisms of PM$_{2.5}$ and are important to validate and improve chemical transport models.

The aerodyne Aerosol Mass Spectrometer (AMS) (Jayne et al., 2000) is a state-of-the-art instrument for measuring size-resolved chemical composition of non-refractory submicron aerosol (NR-PM$_1$) with a high time resolution from seconds to minutes (Jimenez et al., 2003; Allan et al., 2004; Canagaratna et al., 2007). Organic aerosol (OA) measured by the AMS can be further deconvolved into various organic classes from different sources and processes using positive matrix factorization (PMF) (Paatero and Tapper, 1994; Lanz et al., 2010; Ulbrich et al., 2009; Zhang et al., 2011), which has greatly improved our understanding of the key atmospheric processes of OA during the last ten years (Zhang et al., 2007; Jimenez et al., 2009). Based on the AMS system, a simpler instrument, the Quadrupole Aerosol Chemical Speciation Monitor (Q-ACSM), was designed and developed for robust long-term monitoring of the NR-PM$_1$ chemical species (Ng et al., 2011b; Sun et al., 2015). In China, the AMS and Q-ACSM deployments for highly time-resolved chemical evolution processes of NR-PM$_1$ species in urban and rural areas grow rapidly since 2006 (Sun et al., 2010; Huang et al., 2010; Sun et al., 2012a; Hu et al., 2013; Xu et al., 2014; Zhang et al., 2015c; Sun et al., 2016). The new findings and conclusions have been well

summarized in a recent review paper (Li et al., 2017). Secondary organic aerosols (SOA) and secondary inorganic aerosols (e.g., sulfate, nitrate, and ammonium) have been found to be of

75   similar importance in leading to the rapid formation and accumulation of $PM_{2.5}$ during the severe haze events in China (Huang et al., 2014; Sun et al., 2014; Zhang et al., 2014). Recent studies have shown that heterogeneous reactions associated with high anthropogenic NO_x and relative humidity (RH) levels are one of the major formation mechanisms of secondary aerosols, e.g., sulfate (He et al., 2014; Xie et al., 2015; Cheng et al., 2016; Chu et al., 2016; Wang et al., 2016a; Xue et al., 2016).

80   One reason might be that the aqueous oxidation of SO_2 by NO_2 in aerosol water is facilitated by the rich NH_3 which can partly explain the rapid formation of sulfate during severe haze events in China (Wang et al., 2016a). Although the formation mechanisms of sulfate are relatively well understood, the impacts of aerosol water on the formation of SOA in $PM_{2.5}$ remains unclear (Xu et al., 2017b).

85   Limited by the aerodynamic lens, the previous AMS and Q-ACSM only measure aerosol species in PM_1. This is reasonable for the studies in the US and Europe where PM_1 accounts for a large fraction (typically > 70 %) of $PM_{2.5}$ (Sun et al., 2011; Budisulistiorini et al., 2014; Petit et al., 2015). However, a substantial fraction of aerosol particles in 1–2.5 μm ($PM_{1-2.5}$) is frequently observed in China, and the contribution can be more than 50 % during severe haze events (Wang

90   et al., 2015; Zhang et al., 2015b). The source apportionment results of PM_1 might have differences from $PM_{2.5}$ by missing such a large fraction of aerosol particles in $PM_{1-2.5}$. Therefore, instruments which can measure $PM_{2.5}$ composition in real-time are urgently needed in China for a better understanding of variations, sources, and formation mechanisms of $PM_{2.5}$. The techniques for real-time measurements of inorganic species have been well developed, e.g., particle-into-liquid

95   sampler – ion chromatograph (PILS-IC) (Orsini et al., 2003), Monitor for AeRosols and GAses (MARGA) (Du et al., 2011), and Gas and Aerosol Collector – Ion Chromatography (GAC-IC) (Dong et al., 2012), and are also widely used for chemical characterization of $PM_{2.5}$ in China. However, real-time measurements of the total organics in $PM_{2.5}$ and subsequent OA source

apportionment were barely performed in China (Elser et al., 2016). Although ambient organic

100   carbon (OC) and elemental carbon (EC) can be measured semi-continuously, typically in hourly

resolution, they can only be used to differentiate primary and secondary OC using the EC-tracer

technique (Turpin and Huntzicker, 1995). In addition, size-segregated filter samples can provide a

detailed chemical information in different size ranges, but are greatly limited by the sampling

duration, typically days and even weeks (Huang et al., 2014; Xu et al., 2015; Ye et al., 2017).

105   Therefore, real-time characterization of $PM_{2.5}$ is important to have a better understanding of aerosol

chemistry and sources of fine particles in highly-polluted environments in China.

Very recently, a $PM_{2.5}$ lens that can transmit particles larger than 1 μm to the AMS and Q-

ACSM detectors, has been developed and the performance has been fully evaluated in both

laboratories and field studies (Hu et al., 2016; Hu et al., 2017; Xu et al., 2017a). The results showed

110   that the $PM_{2.5}$-Q-ACSM equipped with the new developed capture vaporizer (CV) can detect

approximately 90 % of the $PM_{2.5}$ particles, but more thermal decomposition of both inorganic and

organic species was also observed. Although the CV produces different fragmentation patterns of

organic and inorganic compounds compared with those of a standard vaporizer (SV), it reduces the

particle bouncing effect at the vaporizer and hence improves the quantitative uncertainties caused

115   by collection efficiency (CE). The recent evaluation of the CV for inorganic species measurements

showed overall agreements with those by co-located measurements (Hu et al., 2017). The $PM_{2.5}$-

AMS equipped with a SV was deployed once in China, which provided new insights into

composition and sources of $PM_{2.5}$ in Beijing and Xi'an (Elser et al., 2016). The results showed that

secondary inorganic components (mostly sulfate and nitrate) and oxygenated organic aerosol (OOA)

120   had large enhancements in large sizes (> 1 μm) during the extreme haze periods in Beijing and

Xi'an. It is clear that such real-time measurements of $PM_{2.5}$ composition, particularly for a longer

time with the new CV, in other polluted regions are needed.

In this study, a $PM_{2.5}$-Q-ACSM equipped with a CV was deployed for the first time in the

megacity of Nanjing for the real-time measurement of NR-$PM_{2.5}$ composition. The performance of

125   the PM$_{2.5}$-Q-ACSM is thoroughly evaluated by comparing with measurements by a suite of collocated on-line instruments, including a PM$_1$-Q-ACSM, a Sunset Lab OC/EC Analyzer and a MARGA. The composition, diurnal variations, and processes of aerosol species in NR-PM$_1$ and NR-PM$_{1-2.5}$ are characterized and compared. Moreover, sources of organic aerosols are elucidated by Positive Matrix Factorization (PMF) and new insights into the impacts of aerosol liquid water

130   on the formation of secondary inorganic aerosols and SOA are discussed in this study.

2 Experimental methods

The measurement campaign took place from October 20 to November 16, 2015 in Nanjing, which is a typical mega-city in the western Yangtze River Delta of Eastern China. The sampling site is located at Jiangsu Environment Monitoring Center (32° 02′ 35″ N, 118° 44′ 45″ E),

135   an urban station representative of an atmospheric environment subject to multiple source influences, including industry, traffic, cooking, and biogenic emissions, etc. More detailed descriptions of this sampling site can be found in previous studies (Zhang et al., 2015c; Zhang et al., 2015b; Zhang et al., 2017).

2.1 Instrumentation

140   In this study, two Q-ACSMs, i.e., a PM$_1$-Q-ACSM with SV and a PM$_{2.5}$-Q-ACSM with CV were deployed side by side at the sampling site. The principles of the PM$_1$-Q-ACSM have been detailed elsewhere (Ng et al., 2011b). Briefly, ambient air is sampled into the aerodynamic lens system through a 100 μm diameter critical aperture with a flow rate of ~ 85 cc min^{-1}. The focused particle beam is transmitted through the differentially pumped vacuum chamber into the detection region.

145   Aerosol particles impact and vaporize on an oven at the temperature of approximately 600 °C, and then are ionized with 70 eV electron impact. The produced ions are detected with a quadrupole mass spectrometer (Ng et al., 2011b). Different from the AMS system, the background of the Q-

ACSM is determined by measuring particle-free air.

The differences between the PM_1 and $PM_{2.5}$ Q-ACSMs have been described in Xu et al. (2017a). The three main modifications that enable accurate $PM_{2.5}$ quantification are the sampling inlet, the aerodynamic lens, and the vaporizer. The sampling inlet of the $PM_{2.5}$-Q-ACSM uses straight flow paths and relatively short lengths of tubing to minimize particle loss. The particle lens of the $PM_{2.5}$-Q-ACSM operates at a higher pressure than that of the PM_1-Q-ACSM (Liu et al., 2007; Ng et al., 2011b) and transmits larger particles (Peck et al., 2016; Xu et al., 2017a). And the standard vaporizer is replaced with the capture vaporizer to eliminate the effect of particle bounce which can lead to a fraction of the particle mass not being detected, an effect which increases at larger particle diameters (Hu et al., 2016; Xu et al., 2017a). The PM_1 and $PM_{2.5}$ Q-ACSM mass spectra were analyzed using the Q-ACSM Local toolkit (Version 1.5.11.2), a data analysis software written in Wavemetrics Igor Pro™. The detailed procedures for the data analysis have been described in Ng et al. (2011b) and Sun et al. (2012a). The sensitivity of the two Q-ACSMs were calibrated using size-selected ammonium nitrate (NH_4NO_3) particles (300 nm), which were 1.09×10^{-10} and 2.06×10^{-11}, respectively, for the PM_1 and the $PM_{2.5}$-Q-ACSM. The relative ionization efficiencies (RIEs) of ammonium and sulfate were determined as 4.9 and 4.7, and 0.8 and 1.2 for the PM_1-Q-ACSM and $PM_{2.5}$-Q-ACSM respectively. The default RIE values of 1.1, 1.4, and 1.3 were used for nitrate, organics, and chloride, respectively (Canagaratna et al., 2007; Ng et al., 2011b). In addition, the composition-dependent CE, that is CE = max (0.45, 0.0833 + 0.9167 × ANMF) (Middlebrook et al., 2012), in which ANMF is the mass fraction of ammonium nitrate, was used for the mass concentration quantification of the PM_1-Q-ACSM species, while a CE = 1 was used for the $PM_{2.5}$-Q-ACSM (Xu et al., 2017a).

Water-soluble inorganic ions (NH_4^+, Na^+, K^+, Ca^{2+}, Mg^{2+}, SO_4^{2-}, NO_3^-, and Cl^-) in $PM_{2.5}$ were simultaneously measured by a MARGA at 1 h resolution (Trebs et al., 2004; Rumsey et al., 2014). Ambient air was pulled into the MARGA sampling box with a flow rate of 16.7 L min^{-1}. After removing the interferences of water-soluble gases by a wet rotating denuder, aerosol particles were

dissolved into the liquid phase, and then analyzed with two ion chromatographic systems (Metrohm

175   USA, Inc., Riverview, FL, USA). In addition, the mass concentrations of OC and EC in $PM_{2.5}$ were

measured on a 1hr-basis using a Sunset Lab. Semi-Continuous OCEC Analyzer (Model-4)

implemented with the standard 'abbreviated' NIOSH 5040 thermal protocol (as detailed in Table

S1). A denuder was placed in the sampling line to remove volatile organic compounds and avoid

positive sampling artefacts.

180   The particle number size distribution (3 nm–10 μm) was measured by a Twin Differential

Mobility Particle Sizer (TDMPS, TSI Model 3081) combined with an Aerodynamic Particle Sizer

(APS, TSI Model 3320). The TDMPS consists of two subsystems measuring different size ranges

of dry particles at the same time. The 3–20 nm particles were measured by an Ultrafine Differential

Mobility Analyzer (TSI Model 3085) in conjunction with an Ultrafine Condensation Particle

185   Counter (TSI Model 3025) and the 20–900 nm particles were measured by a Differential Mobility

Analyzer combined with a Condensation Particle Counter (TSI Model 3010). Large particles

between 900 nm and 10 μm were measured by the APS.

Other collocated measurements included the total PM_1 and $PM_{2.5}$ mass concentrations by a

Met one BAM 1020 and a $PM_{2.5}$ Tapered Element Oscillating Microbalance equipped with a Filter

190   Dynamic Measurement System (TEOM-FDMS, Thermo), respectively, and the gaseous species of

CO (model 48i), NO/NO_2 (model 42i), O_3 (model 49i), SO_2 (model 43i), and NH_3 (model 17i) by

Thermo Scientific gas analyzers. Meteorological parameters, including wind speed (WS), wind

direction (WD), ambient temperature (T) and RH, and the parameters of solar radiation (SR) and

precipitation were measured at the same sampling site.

195   **2.2 Q-ACSM data analysis**

PMF analysis of the PM_1 and $PM_{2.5}$ Q-ACSM organic mass spectra was performed within an Igor

Pro-based PMF Evaluation Tool (Ulbrich et al., 2009) with the PMF2.exe algorithm (Paatero and

Tapper, 1994). Pretreatment of the data and error matrices was similar to that reported in previous

studies (Ulbrich et al., 2009; Zhang et al., 2011; Sun et al., 2012b). In addition, $m/z = 12$ and $m/z >$

200   100 were removed in both Q-ACSMs' organic PMF analysis considering (1) a lot of negative values

at m/z 12 due to background uncertainties; (2) a small contribution of $m/z > 100$ in the total organic

signal (Ng et al., 2011b) and large uncertainties due to low ion transmission efficiency and

interference from the internal standard naphthalene signals (Sun et al., 2012a). The PMF results

were evaluated following the procedures detailed in Zhang et al. (2011). The detailed key

205   diagnostic plots for the PMF solution of PM_1 and $PM_{2.5}$ Q-ACSMs are shown in Figs. S1–S4 in the

supporting information. For a better comparison, a simplistic PMF solution was used to extract two

factors, a primary organic aerosol (POA) factor and a SOA factor for both PM_1 and $PM_{2.5}$ Q-

ACSMs. However, a higher order factor analysis utilizing PMF and the multilinear engine (ME-2)

(Canonaco et al., 2013) may reveal more chemical information which should be the subject of a

210   future manuscript.

2.3 Aerosol pH and ALWC prediction

The aerosol pH and liquid water content (ALWC) associated with inorganic species in PM_1 and

$PM_{2.5}$ were predicted using the "forward" mode of ISORROPIA-II (Fountoukis and Nenes, 2007),

with both inorganic composition and gas-phase species (HNO_3 and NH_3) as model inputs. To

215   investigate the potential influence of mineral dust and sea salts, as well as the differences of aerosol

chemical species measured by different instruments on the pH prediction, the model was also run

with and without K^+–Ca^{2+}–Mg^{2+} or Na^+–Cl^-, respectively. The predicted aerosol pH is defined as

in equation (1):

$$pH = -\log_{10} H_{aq}^+ = -\log_{10} \frac{1000 H_{air}^+}{ALWC} \qquad (1)$$

220   where H_{aq}^+ (mol L^{-1}) is the hydronium ion concentration in ALWC driven by inorganic aerosols.

H_{air}^+ (µg m^{-3}) is the hydronium ions concertation per volume air. The predicted NH_3 by

ISORROPIA-II agreed well with the measured NH_3 (Fig. S5), suggesting that the aerosol phase

state was representative via the thermodynamic analysis. Figure S6 presents the time series of pH

for PM_1 and $PM_{2.5}$. By excluding mineral dust and sea salt species in ISORROPIA-II, the predicted

225   pH was in the range of 1.23 – 4.19 (PM_1-Q-ACSM), 1.78 – 4.10 ($PM_{2.5}$-Q-ACSM), and 1.98 – 4.07

($PM_{2.5}$-MARGA), with the mean values being 3.47, 3.33, and 3.42, respectively. The aerosol pH

showed slight increases by 5 – 6 % except for the dust-related period if crustal species were

included (Fig. S7). This indicates that the aerosol pH prediction was generally consistent with the

measurements from different instruments. However, the crustal species have large impacts on the

230   aerosol pH. For example, the fine aerosol pH shows an evident increase from 2.8 – 3.03 to 3.7

during the dust period after the cations of Ca^{2+}, Mg^{2+}, and K^+ were included. Figure S8 shows

excellent agreements of pH prediction with and without Na^+ and Cl^- as the model inputs, suggesting

the negligible influence of sea salts on aerosol particle acidity in this study. One reason is the

relatively low concentrations of Na^+ (0 – 0.87 µg m^{-3}) during the campaign.

3 Results and discussion

3.1 Inter-comparisons

As shown in Fig. 1, the mass concentrations of PM_1 and $PM_{2.5}$ measured by the Q-ACSMs agree

well with those measured by collocated instruments (i.e., the total PM mass analyzers, including

TEOM-FDMS and BAM-1020) and those estimated from size-resolved particle number

240   concentrations (TDMPS and APS) and the composition dependent particle density (Fig. S9). On

average, the total dry mass of PM_1 and $PM_{2.5}$ Q-ACSM reports 89 % and 93 % of the volume-

dependent mass, respectively (Fig. S10). As reported in Xu et al. (2017a), the $PM_{2.5}$ lens system

might have a considerable loss for particles below 200 nm due to the lens transmission efficiency

(on average 45 %), which can partly explain the differences between the Q-ACSM and TDMPS

245   (Fig. S10d). The NR-$PM_{2.5}$ concentrations report approximately 90 % of the total $PM_{2.5}$

concentrations measured by the TEOM-FDMS and/or BAM 1020 instruments. After considering

the contributions of EC and alkaline cations ($Na^+ + K^+ + Ca^{2+} + Mg^{2+}$), it can explain 92 % of the $PM_{2.5}$ mass. This slight underestimation of the total $PM_{2.5}$ mass might be primarily due to discrepancies between the different inlet cut-offs, measurement uncertainties of the different

250 instruments, and, as further discussed below, the un-identified mineral dust and sea salt components. Figures 2 and 3 show the inter-comparisons of the measurements by the $PM_{2.5}$-Q-ACSM with those by other co-located instruments, including the PM_1-Q-ACSM, MARGA, and OC/EC analyzer. Overall, the $PM_{2.5}$-Q-ACSM measurements are well correlated with those measured by co-located instruments ($r^2 > 0.9$), except for chloride. SNA (= sulfate + nitrate + ammonium) measured by the

255 $PM_{2.5}$-Q-ACSM were highly correlated with those measured by the MARGA ($r^2 = 0.92$–0.95). The absolute agreement between the $PM_{2.5}$-Q-ACSM and MARGA is very good for sulfate (slope = 1.02). The ammonium agreement is also quite good with the $PM_{2.5}$ Q-ACSM measuring on average 89 % of that reported by the MARGA. The average ratios of the measured NH_4^+ to predicted NH_4^+ that require to fully neutralize SO_4^{2-}, NO_3^-, and Cl^- were 1.02 and 0.95 for the $PM_{2.5}$-Q-ACSM and

260 PM_1-Q-ACSM, respectively (Fig. S11), which is similar to the water-soluble ion balance results from the MARGA (Fig. S12). For nitrate, however, the $PM_{2.5}$ Q-ACSM measures about 68 % of what is reported by the MARGA. One reason might be due to the contribution of nitrate from aged sea salts and/or mineral dust (e.g., $NaNO_3$ and $Mg(NO_3)_2$) (Gibson et al., 2006), which the Q-ACSM cannot detect due to the limited vaporizer temperature. The much lower ratio of chloride

265 (0.26, Fig. 3f) between the $PM_{2.5}$-Q-ACSM and MARGA also suggests the presence of such sea salt and/or crustal particles. As shown in Fig. S13a, we estimated that about 83 % of the difference between the chloride $PM_{2.5}$-Q-ACSM and MARGA measurements could be explained by a maximum estimate of refractory chloride calculated using the ion mass balance with Na^+, Ca^{2+}, K^+, and Mg^{2+}. In addition, this estimated maximum refractory-chloride concentration also shows a

270 positive relationship ($r^2 = 0.36$) with the difference between the nitrate loadings obtained from the $PM_{2.5}$-Q-ACSM and MARGA (Fig. S13b). The presence of refractory-chloride (-nitrate) may then explain a large fraction of the discrepancies observed for these species between both $PM_{2.5}$

chemical analyzers. Moreover, a recent evaluation of the AMS with a CV system also found a large difference in chloride measurements (Hu et al., 2017), yet the reason was not completely understood. A future RIE calibration for chloride in the CV system might be helpful to evaluate these differences.

As presented in Fig. 2, organics measured by the PM_1 and $PM_{2.5}$ Q-ACSMs both show good correlations with the OC measured by the OC/EC Analyzer ($r^2 = 0.77$ and 0.93, respectively). The slope obtained between the $PM_{2.5}$ measurements, that is the $PM_{2.5}$ organic mass-to-organic carbon (OM / OC) ratio, is however relatively high, considering either the so-called "thermal OC" or "optical OC" Sunset measurements (i.e., 3.5 and 2.9 respectively), as shown in Fig. 3b. Indeed, most of the previous studies generally reported a ratio below 2.5 for aged submicron OA (e.g., Aiken et al., 2008; Zhang et al., 2011). Nevertheless, the 2.9 and 3.5 values obtained here are close to values reported in a few other studies, e.g., a ratio of 3.3 observed in Pasadena (Hayes et al., 2013), and it may be expected that $PM_{1-2.5}$ organic aerosols may be more oxidized than the submicron fraction (with a higher contribution of SOA, as discussed in section 3.2.2), and therefore have somewhat higher OM / OC ratios than those in NR-PM_1. Moreover, in the AMS and Q-ACSM systems, the fraction of OA signal at m/z 44 (f_{44}), mostly dominated by CO_2^+, is commonly considered as a surrogate of atomic oxygen-to-carbon (O / C) and OM / OC (Aiken et al., 2008; Ng et al., 2011a). As reported from the ACTRIS Q-ACSM inter-comparison works, instrument artefacts may significantly affect the variability in f_{44} measured by different Q-ACSMs (Crenn et al., 2015). For example, Pieber et al. (2016) recently found that thermal decomposition products of inorganic salts on the SV may raise up the non-OA CO_2^+ signal, which can increase f_{44} values. Therefore, the impact of instrument artefacts on the $PM_{2.5}$-Q-ACSM should be also investigated in a future study. Another reason for this discrepancy is likely that OC is underestimated by the Sunset OC/EC analyzer due to evaporative loss of semi-volatile organic carbon during the sampling (Bae et al., 2006; Sun et al, 2011). It is also possible that large particles are not being efficiently delivered to the filter in the semi-continuous OC/EC analyzer as they pass through a warm solenoid valve

with a bent flow path upstream of the filter.

Figure 3 also shows that SNA measured by the PM_1-Q-ACSM were tightly correlated with those measured by the MARGA ($r^2 = 0.68$–0.87), indicating that the temporal variations of inorganic species in NR-PM_1 are generally similar to those in $PM_{2.5}$. However, the SNA in NR-PM_1 only report 25–49 % of those in $PM_{2.5}$, indicating that a large fraction of SNA is present in the size range of 1–2.5 μm (NR-$PM_{1-2.5}$). As shown in Fig. S14, the average ratio of NR-PM_1 to NR-$PM_{2.5}$ is 0.48, suggesting that nearly half of NR-$PM_{2.5}$ is NR-$PM_{1-2.5}$. This is quite different from the results observed in the US and Europe that a dominant fraction of $PM_{2.5}$ is PM_1 (Sun et al., 2011; Petit et al., 2015). For instance, 91 % of $PM_{2.5}$ nitrate was found in NR-PM_1 at an urban background site in Paris, France (Petit et al., 2015). Our results indicate that it is of great importance to chemically characterize $PM_{1-2.5}$ in China because of its large contribution to the total mass of $PM_{2.5}$ in accordance with Elser et al. (2016). Figure 4 shows the relationship between the $PM_1/PM_{2.5}$ ratios of the aerosol species from the Q-ACSM measurements and the ratio of SOA to OA in $PM_{2.5}$. It can be seen that the ratios of all aerosol species generally decrease with the increase of SOA/OA in $PM_{2.5}$. Given that primary particles are more abundant than SOA in smaller size ranges, our results suggest that the $PM_{2.5}$ CV and PM_1 SV Q-ACSMs show a better agreement for measuring smaller particles while larger particles have higher probability to bounce off the SV surface compared with the CV (Xu et al., 2017a).

3.2 Sized-segregated investigation of NR-$PM_{2.5}$ components

Figure 5 presents the time series of the mass concentrations of the NR-PM_1 and NR-$PM_{2.5}$ species, meteorological parameters, gas-phase species and size-resolved particle number concentrations for the entire study. The entire study period was characterized by five episodes (Ep1–Ep5) according to different pollution events as marked in Fig. 5e. The mass concentrations of the total NR-PM_1 and NR-$PM_{2.5}$ vary dramatically throughout the entire study, ranging from 4.2 to 81.9 μg m^{-3}, and

9.3 to 178.7 μg m^{-3}, respectively. For example, aerosol mass loadings increase rapidly from a few μg m^{-3} to hundreds of μg m^{-3} within a short-time scale, e.g., Ep2, Ep4, and Ep5, which are associated with new particle formation and growth (Ep2) and foggy days (Ep4 and Ep5), respectively (Fig. 5e). We also noticed that such rapid changes in aerosol mass were generally associated with a wind direction change to the northwest (Fig. 5a). This result indicates the potential source contributions in the northwest region to the PM level in Nanjing. The average NR-PM$_1$ and NR-PM$_{2.5}$ were 32.5 μg m^{-3} and 68.7 μg m^{-3}, respectively, for the entire study, indicating that 53 % of the PM$_{2.5}$ mass is in the size range of 1–2.5 μm. During the persistent pollution events, e.g., Ep1 and Ep2, NR-PM$_{1-2.5}$ accounts for 56 % and 42 % of the total NR-PM$_{2.5}$. Overall, NR-PM$_{1-2.5}$ also shows a ubiquitously higher contribution to NR-PM$_{2.5}$ than that of NR-PM$_1$ during different types of episodes, except Ep3, further highlighting the importance for characterization of aerosol particles between 1 and 2.5 μm.

3.2.1 Secondary inorganic aerosols

SNA constitutes a major fraction of NR-PM$_{2.5}$, on average accounting for 61 % in this study (Fig. 6). The average mass concentrations of SNA in NR-PM$_1$ and NR-PM$_{2.5}$ were 19.6 μg m^{-3} and 40.6 μg m^{-3}, respectively, both of which are about 1.6–1.7 times higher than that of organics. The average mass concentration of sulfate in NR-PM$_1$ is 5.9 μg m^{-3}, which is close to that (5.4 μg m^{-3}) measured by a soot particle (SP) AMS during springtime in urban Nanjing (Wang et al., 2016b). However, it is nearly 3 times lower than that in NR-PM$_{2.5}$ (17.4 μg m^{-3}) indicating that a major fraction of sulfate exists in the size range of 1–2.5 μm. Sulfate frequently comprises the largest fraction of NR-PM$_{1-2.5}$ with SOA being the second largest, particularly in the polluted episodes (Fig 6b). On average, sulfate and SOA contribute 33 % and 30 % to the total NR-PM$_{1-2.5}$, respectively, during the entire period. Sulfate accounts for the largest contribution (41 %) to the

total NR-PM$_{1-2.5}$ loading during the persistent pollution event (Ep1). Compared with sulfate (26 %), nitrate accounts for a lower fraction (19 %) of NR-PM$_{2.5}$ for the entire study, and the contribution to NR-PM$_{1-2.5}$ is typically 2–4 times lower than that to NR-PM$_1$. One reason is likely that non-refractory nitrate (e.g., ammonium nitrate) mainly existed in submicron aerosols, while that in NR-PM$_{1-2.5}$ contains more nitrate from sea salt and mineral dusts.

In addition, the average aerosol pH was 3.59 ± 0.37 and 3.51 ± 0.39, respectively using the PM$_{2.5}$ MARGA and PM$_{2.5}$-Q-ACSM measurements as ISORROPIA-II inputs (Fig. 7), indicative of acidic aerosol particles in this study. The pH values here are consistent with that (average = 4.2) observed during haze episodes in Beijing (Liu et al., 2017). Recent studies showed that sulfate formation was more sensitive to aqueous oxidation of SO$_2$ in the presence of high NO$_2$ and neutral conditions during the haze pollution periods in China (Cheng et al., 2016; Wang et al., 2016a). However, the pH values observed in this study suggest acidic particles, indicating that the aqueous oxidation pathway of SO$_2$ by NO$_2$ to form sulfate was not favored during the haze episodes in this study.

3.2.2 POA and SOA

The average mass concentration of OA in NR-PM$_{2.5}$ (25.2 µg m^{-3}) is approximately twice that in NR-PM$_1$ (11.3 µg m^{-3}). Despite the large differences in mass concentrations, the contributions of organics to the total NR-PM$_{1-2.5}$ and NR-PM$_1$ are relatively similar (40 % vs. 36 %). POA on average contributes 34 % to the total OA in NR-PM$_1$, which is higher than the contribution (28 %) in NR-PM$_{2.5}$ during the entire study. In contrast, SOA showed a higher fraction in OA in NR-PM$_{2.5}$ (72 %) than NR-PM$_1$ (66 %). As shown in Fig. 6, the mass concentrations (9.0–11.8 µg m^{-3}) and mass fractions (14–20 %) of SOA in NR-PM$_{1-2.5}$ are also ubiquitously higher than those in NR-PM$_1$ (4.3–10.4 µg m^{-3}, and 10–13 %).

Figure 8a shows a comparison of the mass spectra of POA and SOA between NR-PM$_1$ and

NR-PM$_{2.5}$. While the mass spectra were overall similar, the one resolved from the PM$_{2.5}$-Q-ACSM

370   with capture vaporizer showed higher contributions of small m/z's. This is consistent with the

recent findings that the CV is subject to have enhanced thermal decomposition compared to the SV

(Hu et al., 2016). Similar to previous studies, the POA spectrum is characterized by the typical

hydrocarbon ion series C$_n$H$_{2n-1}^+$ and C$_n$H$_{2n+1}^+$ (Zhang et al., 2011), e.g., m/z 55 and m/z 57, as well

as AMS biomass-burning tracers (Alfarra et al., 2007), e.g., m/z 60 and m/z 73. Note that the mass

375   spectra of NR-PM$_{2.5}$ show smaller fractions of m/z 60 and m/z 73 signals, compared with those of

PM$_1$ (Fig. 8a and Fig. S15), which is likely due to the stronger thermal decomposition (Pieber et al.,

2016). The high ratio of m/z 55/57 (1.91) in the SV system suggests a significant influence from

local cooking emissions (Allan et al., 2010; Mohr et al., 2012; Sun et al., 2012a; Zhang et al.,

2015c). In addition to the noon and evening meal time peaks, the diurnal variations of POA in Fig.

380   S16 also show two peaks corresponding to morning rush hours (Zhang et al., 2015b), and night

biomass-burning emissions (Zhang et al., 2015c). This result suggests that the POA factor in this

study is subject to multiple influences, including traffic, cooking, and biomass burning emissions.

The mass spectrum of SOA in both NR-PM$_1$ and NR-PM$_{2.5}$ is dominated by m/z 44 (mostly CO$_2^+$)

with a higher f_{44} in the NR-PM$_{2.5}$ system. One reason for the higher f_{44} in the PM$_{2.5}$-Q-ACSM could

385   be the effects of enhanced thermal decomposition in the CV system (Xu et al., 2017a). Another

possibility is the more crustal materials in PM$_{1-2.5}$ which can produce a non-OA CO$_2^+$ interference

signal from the reactions on the particle SV (Pieber et al., 2016; Bozzetti et al., 2017). For example,

the deposited carbonates on the particle vaporizer in the AMS/Q-ACSM system may release a CO$_2^+$

signal upon reaction with HNO$_3$ and NO$_x$ (Goodman et al., 2000; Pieber et al., 2016). In addition,

390   as discussed in Sect. 3.1, the instrument artefacts may lead to the f_{44} discrepancies among different

Q-ACSM instruments and thereby affect factor profiles in the ME-2/PMF analysis (Fröhlich et al., 2015), which might also have a potential impact on the PMF analysis of PM$_{2.5}$-Q-ACSM OA mass spectra in this study.

SOA shows a positive relationship with ALWC, and the slope ratio of SOA to ALWC is strongly dependent on the RH levels (Fig. 9a). For example, the ratios at low RH levels (RH < 40 %) (2.25 and 2.50 in PM$_1$ and PM$_{2.5}$, respectively) are much higher than those at high RH levels (RH > 80 %, slope = 0.18 and 0.22). Figure 10 presents results obtained from the nonparametric wind regression analysis performed following the procedures described in Petit et al. (2017). High RH levels (> 80 %) and ALWC (> 30 µg.m^{-3} for PM$_1$ and 50 µg.m^{-3} for PM$_{2.5}$) are mainly associated with Northwestern air masses, the latter ones being loaded with relatively high amounts of secondary aerosols (SOA, as well as nitrate and sulfate) but low amount of gas-phase precursors (e.g., O$_3$, SO$_2$, NO$_2$, and NH$_3$). These results suggest the predominance of aqueous phase chemistry in SOA formation from the Northwestern sector. Moreover, as shown in Fig. 9b, SOA correlates well with [SO$_4^{2-}$ + NO$_3^-$] (r^2 = 0.72 and 0.75 for NR-PM$_1$ and NR-PM$_{2.5}$, respectively), and the correlation coefficient shows an evident RH dependence with a stronger correlation at high RH levels (e.g., RH > 80 %, r^2 = 0.92). This suggests that SOA might be well internally mixed with SNA, and the enhancement of SOA might be caused by aqueous-phase chemistry under high RH levels in urban Nanjing. In addition, the ratio of SOA to [SO$_4^{2-}$ + NO$_3^-$] is also dependent on RH, with higher slopes (0.58 and 0.75 for NR-PM$_1$ and NR-PM$_{2.5}$, respectively) at RH < 40 % and lower values at RH > 80 (0.41 and 0.50, respectively), suggesting that the enhancement of SNA was higher than the SOA production via aqueous-phase chemistry pathways. High SOA at low RH levels was likely mainly from photochemical production, which is also supported by the

correspondingly high O_x (= O_3 + NO_2) levels (Fig. 9c). Figure 9c also shows that the SOA

concentrations in both PM_1 and $PM_{2.5}$ increase with the increase of O_x, and the ratios of SOA to O_x

show clear enhancements as the RH levels increase. For example, the ratio of [NR-PM_1 SOA] /

[O_x] at low RH conditions (RH < 50 %) is close to that observed in our previous study during a

period with strong photochemical processing (Zhang et al., 2017). The mass spectra of OA are also

substantially different between low and high RH and/or O_x levels (Fig. S17). For instance, the mass

spectra of SOA in both NR-PM_1 and NR-$PM_{2.5}$ were characterized by higher signals at *m/z* 44 at

high RH levels, likely suggesting the formation of more oxidized SOA via aqueous processing (Xu

et al., 2017b). These results might indicate that the total SOA contains different types of SOA at

low and high RH levels. While the formation of SOA at high RH levels is significantly affected by

aqueous-phase processing, it might be driven more by photochemical processing at low RH levels.

3.4 Specific episodes analysis (Ep2 and Ep5)

Figure 11 shows the temporal variation of secondary aerosols, including SOA and SNA, in NR-

PM_1 and NR-$PM_{1-2.5}$ during two different episodes. A clear particle nucleation and growth event

was observed before the formation of the first episode (Ep2, Fig. 11a), during which the air was

relatively clean ($PM_{2.5}$ mass loading = 28.5 μg m^{-3}) and SR was strong (610.5 W m^{-2}). The number

concentration of nucleation mode particles increased rapidly from ~ 670 to 2400 (# cm^{-3}) within 1

hour, and the particle size grew from ~ 3 nm to 100 nm during the rest of the day. The role of new

particle formation and growth in the formation of haze pollution has been reported in urban

environments (Guo et al., 2014). Here, we observed simultaneous increases in secondary aerosol

species (Fig. 11a) and gaseous NH_3 and SO_2 during the particle growth period (Fig. 5d).

435 Comparatively, NO_x shows a pronounced night peak and then decreases rapidly during daytime because it is mainly from local traffic emissions (Fig. 5d). Interestingly, the aerosol pH shows an evident peak (pH = ~4) during the new particle formation (Fig. 11a), while ALWC is very low (2.4 $\mu g \ m^{-3}$). This suggests that heterogeneous reactions might be involved into the new particle formation process under such NH_3-rich environments. Although only one such case was observed

440 throughout the entire study due to the suppression of new particle formation by abundant preexisting particles under the polluted environments, it appears that the continuous growth from nucleation mode particles under abundant NH_3, SO_2, and NO_x might also be one of the reasons for the high PM pollution in Nanjing.

The formation of secondary aerosol was more rapid during Ep5 compared to Ep2 (Fig. 11b),

445 and was clearly associated with a fog event (RH > 80 % and averaged ALWC = 53.9 $\mu g \ m^{-3}$). While the number concentration of Aitken mode particles remained small, the mass concentrations of secondary sulfate, nitrate and SOA showed dramatic increases along with simultaneous increases in large particles (D_m > 100 nm) and aerosol pH (Fig. 11b). This is likely due to the efficient uptake kinetics of gaseous species (e.g., SO_2, NO_2, and NH_3) upon preexisting aerosol water (Cheng et al.,

450 2016; Xue et al., 2016), which may undergo aqueous/heterogeneous reactions and subsequent hygroscopic growth at high RH. In fact, the mass fractions of secondary species of NR-$PM_{1–2.5}$ in $PM_{2.5}$ increased from 33 % to 56 %. These results support that aqueous processing plays a more important role in haze formation under high RH conditions and that it tends to form more large particles. The enhancement of SOA production via aqueous-phase chemistry has been observed in

455 many previous field studies (Ge et al., 2012; Chakraborty et al., 2015; Sun et al., 2016). As

discussed above, SOA in this study shows a good correlation with $[SO_4^{2-} + NO_3^-]$ and particle

water (under high RH levels), indicating that aqueous chemistry during foggy days might facilitate

the production of both SNA and SOA (Sun et al., 2013; Xu et al., 2017b). We also compared the

OA mass spectra between the two episodes. The OA mass spectra during the fog episode were

460   characterized by much higher m/z 44 and f_{44} compared with those during the new particle formation

episode (Fig. S17). This result indicates different formation mechanisms of SOA between the two

different episodes. Chakraborty et al. (2015) have also observed similar aerosol composition

differences between foggy and non-foggy events with a high-resolution aerosol mass spectrometer

instrument deployed in Kanpur, India. While photochemical processing is the major formation

465   mechanism of Ep2, aqueous-phase processing is more important for the formation of more aged

SOA.

4 Conclusions and Implications

The chemically-resolved mass concentration of NR-PM$_{2.5}$ was measured in-situ by the newly

470   developed PM$_{2.5}$-Q-ACSM in urban Nanjing, China for the first time. The measured NR-PM$_{2.5}$

chemical species (organics, sulfate, ammonium, and nitrate) correlated well ($r^2 > 0.9$) with those

from co-located measurements by the MARGA and OC/EC Analyzer. Also, all NR-PM$_{2.5}$ species

were tightly correlated with those in NR-PM$_1$ that were measured by a PM$_1$-Q-ACSM. The

comparisons between the two different Q-ACSMs revealed substantial mass fractions of aerosol

475   species in NR-PM$_{1-2.5}$, yet the ratios of [NR-PM$_1$] / [NR-PM$_{2.5}$] varied among different species. In

particular, nitrate and chloride showed much higher [NR-PM$_1$] / [NR-PM$_{2.5}$] ratios compared with

other species. The reasons are not very clear yet although refractory mineral dust and sea salts can

explain some differences. However, such difference here had an insignificant influence on aerosol pH prediction. The PMF analysis also showed similar temporal variations in POA and SOA between NR-PM$_1$ and NR-PM$_{2.5}$, but the mass spectra were slightly different with higher f_{44} and more small fragments for OA in NR-PM$_{2.5}$ due to enhanced thermal decomposition.

On average, NR-PM$_{2.5}$ was mainly composed of SOA (27 %) and SNA (61 %) for the entire study, of which 16 % of SOA and 17 % of sulfate were present in the size range of 1–2.5 µm. A high aerosol pH peak and a low ALWC was observed during the new particle formation process, suggesting that heterogeneous reactions in the presence of NH$_3$ might promote the new particle formation and hereafter growth processes in urban areas in eastern China. Fog case analysis showed that secondary aerosol species (SNA and SOA) in NR-PM$_{1-2.5}$, aerosol pH and ALWC showed rapid increases within several hours during the fog processing which also contributed the dominant fractions of the total PM$_{2.5}$ mass while smaller particles (less than 100 nm) remained relatively unchanged, indicating an enhanced role of aerosol species in PM$_{1-2.5}$ during the fog episode. These results suggest that the increased aqueous aerosol surface may enhance SOA production via heterogeneous reactions. Therefore, decreasing anthropogenic NO$_2$, SO$_2$, and NH$_3$ emissions may reduce both SNA and SOA levels. Overall, our study highlights the importance of real-time characterization of the PM$_{2.5}$ composition to study the sources and processes of fine particles in China.

Data availability. The observational data in this study are available from the authors upon request (lily3258@163.com).

Competing interests. The authors declare that they have no conflict of interest.

Acknowledgments. This work was supported by the Natural Science Foundation of China (D0512/91544231, 41575120) and the National Key Research and Development Plan of China

(2016 YFC0200505). The development of the PM$_{2.5}$-ACSM was funded by US EPA grant # EP-D-

505   12-007 and US DoE grant # DE-SC0001673. We would like to thank Dr. Ping Chen for his support

in this campaign. Yunjiang Zhang acknowledges a PhD Scholarship from the China Scholarship

Council (CSC).

References

510   Aiken, A. C., DeCarlo, P. F., Kroll, J. H., Worsnop, D. R., Huffman, J. A., Docherty, K. S., Ulbrich, I. M., Mohr, C., Kimmel, J. R., Sueper, D., Sun, Y., Zhang, Q., Trimborn, A., Northway, M., Ziemann, P. J., Canagaratna, M. R., Onasch, T. B., Alfarra, M. R., Prevot, A. S. H., Dommen, J., Duplissy, J., Metzger, A., Baltensperger, U., and Jimenez, J. L.: O/C and OM/OC ratios of primary, secondary, and ambient organic aerosols with high-resolution time-of-flight aerosol

515   mass spectrometry, Environ. Sci. Technol., 42, 4478-4485, 10.1021/es703009q, 2008.

Alfarra, M. R., Prevot, A. S. H., Szidat, S., Sandradewi, J., Weimer, S., Lanz, V. A., Schreiber, D., Mohr, M., and Baltensperger, U.: Identification of the mass spectral signature of organic aerosols from wood burning emissions, Environ. Sci. Technol., 41, 5770-5777, 10.1021/es062289b, 2007.

520   Allan, J. D., Delia, A. E., Coe, H., Bower, K. N., Alfarra, M. R., Jimenez, J. L., Middlebrook, A. M., Drewnick, F., Onasch, T. B., Canagaratna, M. R., Jayne, J. T., and Worsnop, D. R.: A generalised method for the extraction of chemically resolved mass spectra from Aerodyne aerosol mass spectrometer data, J. Aerosol Sci., 35, 909-922, 10.1016/j.jaerosci.2004.02.007, 2004.

525   Allan, J. D., Williams, P. I., Morgan, W. T., Martin, C. L., Flynn, M. J., Lee, J., Nemitz, E., Phillips, G. J., Gallagher, M. W., and Coe, H.: Contributions from transport, solid fuel burning and cooking to primary organic aerosols in two UK cities, Atmos. Chem. Phys., 10, 647-668, 10.5194/acp-10-647-2010, 2010.

Bae, M.-S., Demerjian, K. L., and Schwab, J. J.: Seasonal estimation of organic mass to organic
530   carbon in $PM_{2.5}$ at rural and urban locations in New York state, Atmos. Environ., 40 (39): 7467-7479, 2006.

Bozzetti, C., El Haddad, I., Salameh, D., Daellenbach, K. R., Fermo, P., Gonzalez, R., Minguillón, M. C., Iinuma, Y., Poulain, L., Müller, E., Slowik, J. G., Jaffrezo, J. L., Baltensperger, U., Marchand, N., and Prévôt, A. S. H.: Organic aerosol source apportionment by offline-AMS

535   over a full year in Marseille, Atmos. Chem. Phys. Discuss., 2017, 1-46, 10.5194/acp-2017-54, 2017.

Budisulistiorini, S. H., Canagaratna, M. R., Croteau, P. L., Baumann, K., Edgerton, E. S., Kollman, M. S., Ng, N. L., Verma, V., Shaw, S. L., Knipping, E. M., Worsnop, D. R., Jayne, J. T., Weber, R. J., and Surratt, J. D.: Intercomparison of an Aerosol Chemical Speciation Monitor (Q-

540   ACSM) with ambient fine aerosol measurements in downtown Atlanta, Georgia, Atmos. Meas. Tech., 7, 1929-1941, 10.5194/amt-7-1929-2014, 2014.

Canagaratna, M. R., Jayne, J. T., Jimenez, J. L., Allan, J. D., Alfarra, M. R., Zhang, Q., Onasch, T. B., Drewnick, F., Coe, H., Middlebrook, A., Delia, A., Williams, L. R., Trimborn, A. M., Northway, M. J., DeCarlo, P. F., Kolb, C. E., Davidovits, P., and Worsnop, D. R.: Chemical and

545   microphysical characterization of ambient aerosols with the aerodyne aerosol mass spectrometer, Mass Spectrom. Rev., 26, 185-222, 10.1002/mas.20115, 2007.

Canonaco, F., Crippa, M., Slowik, J. G., Baltensperger, U., and Prévôt, A. S. H.: SoFi, an IGOR-based interface for the efficient use of the generalized multilinear engine (ME-2) for the source apportionment: ME-2 application to aerosol mass spectrometer data, Atmos. Meas. Tech., 6,

550   3649-3661, 10.5194/amt-6-3649-2013, 2013.

Chakraborty, A., Bhattu, D., Gupta, T., Tripathi, S. N., and Canagaratna, M. R.: Real-time measurements of ambient aerosols in a polluted Indian city: Sources, characteristics, and processing of organic aerosols during foggy and nonfoggy periods, J. Geophys. Res. Atmos., 120, 9006-9019, 10.1002/2015JD023419, 2015.

555 Cheng, Y., Zheng, G., Wei, C., Mu, Q., Zheng, B., Wang, Z., Gao, M., Zhang, Q., He, K., Carmichael, G., Pöschl, U., and Su, H.: Reactive nitrogen chemistry in aerosol water as a source of sulfate during haze events in China, Sci. Adv., 2, 10.1126/sciadv.1601530, 2016.

Chu, B., Zhang, X., Liu, Y., He, H., Sun, Y., Jiang, J., Li, J., and Hao, J.: Synergetic formation of secondary inorganic and organic aerosol: effect of SO_2 and NH_3 on particle formation and

560   growth, Atmos. Chem. Phys., 16, 14219-14230, 10.5194/acp-16-14219-2016, 2016.

Crenn, V., Sciare, J., Croteau, P. L., Verlhac, S., Fröhlich, R., Belis, C. A., Aas, W., Äijälä, M., Alastuey, A., Artiñano, B., Baisnée, D., Bonnaire, N., Bressi, M., Canagaratna, M., Canonaco, F., Carbone, C., Cavalli, F., Coz, E., Cubison, M. J., Esser-Gietl, J. K., Green, D. C., Gros, V., Heikkinen, L., Herrmann, H., Lunder, C., Minguillón, M. C., Močnik, G., O'Dowd, C. D., Ovadnevaite, J., Petit, J. E., Petralia, E., Poulain, L., Priestman, M., Riffault, V., Ripoll, A., Sarda-Estève, R., Slowik, J. G., Setyan, A., Wiedensohler, A., Baltensperger, U., Prévôt, A. S. H., Jayne, J. T., and Favez, O.: ACTRIS ACSM intercomparison – Part 1: Reproducibility of concentration and fragment results from 13 individual quadrupole aerosol chemical speciation monitors (Q-ACSM) and consistency with co-located instruments, Atmos. Meas. Tech., 8, 5063-5087, 10.5194/amt-8-5063-2015, 2015.

Ding, A. J., Huang, X., Nie, W., Sun, J. N., Kerminen, V. M., Petäjä, T., Su, H., Cheng, Y. F., Yang, X. Q., Wang, M. H., Chi, X. G., Wang, J. P., Virkkula, A., Guo, W. D., Yuan, J., Wang, S. Y., Zhang, R. J., Wu, Y. F., Song, Y., Zhu, T., Zilitinkevich, S., Kulmala, M., and Fu, C. B.: Enhanced haze pollution by black carbon in megacities in China, Geophys. Res. Lett., 43, 2873-2879, 10.1002/2016GL067745, 2016.

Dong, H. B., Zeng, L. M., Hu, M., Wu, Y. S., Zhang, Y. H., Slanina, J., Zheng, M., Wang, Z. F., and Jansen, R.: Technical Note: The application of an improved gas and aerosol collector for ambient air pollutants in China, Atmos. Chem. Phys., 12, 10519-10533, 10.5194/acp-12-10519-2012, 2012.

Du, H., Kong, L., Cheng, T., Chen, J., Du, J., Li, L., Xia, X., Leng, C., and Huang, G.: Insights into summertime haze pollution events over Shanghai based on online water-soluble ionic composition of aerosols, Atmos. Environ., 45, 5131-5137, , 2011.

Elser, M., Huang, R. J., Wolf, R., Slowik, J. G., Wang, Q., Canonaco, F., Li, G., Bozzetti, C., Daellenbach, K. R., Huang, Y., Zhang, R., Li, Z., Cao, J., Baltensperger, U., El-Haddad, I., and Prévôt, A. S. H.: New insights into $PM_{2.5}$ chemical composition and sources in two major cities in China during extreme haze events using aerosol mass spectrometry, Atmos. Chem. Phys.,

16, 3207-3225, 10.5194/acp-16-3207-2016, 2016.

Fountoukis, C. and Nenes, A.: ISORROPIA II: a computationally efficient thermodynamic equilibrium model for K^+- Ca^{2+} - Mg^{2+} - NH_4^+ - Na^+ - SO_4^{2-} - NO_3^- - Cl^- - H_2O aerosols, Atmos.

590   Chem. Phys., 7, 4639-4659, 10.5194/acp-7-4639-2007, 2007.

Fröhlich, R., Crenn, V., Setyan, A., Belis, C. A., Canonaco, F., Favez, O., Riffault, V., Slowik, J. G., Aas, W., Aijälä, M., Alastuey, A., Artiñano, B., Bonnaire, N., Bozzetti, C., Bressi, M., Carbone, C., Coz, E., Croteau, P. L., Cubison, M. J., Esser-Gietl, J. K., Green, D. C., Gros, V., Heikkinen, L., Herrmann, H., Jayne, J. T., Lunder, C. R., Minguillón, M. C., Močnik, G., O'Dowd, C. D.,

595   Ovadnevaite, J., Petralia, E., Poulain, L., Priestman, M., Ripoll, A., Sarda-Estève, R., Wiedensohler, A., Baltensperger, U., Sciare, J., and Prévôt, A. S. H.: ACTRIS ACSM intercomparison – Part 2: Intercomparison of ME-2 organic source apportionment results from 15 individual, co-located aerosol mass spectrometers, Atmos. Meas. Tech., 8, 2555-2576, 10.5194/amt-8-2555-2015, 2015.

600 Ge, X., Zhang, Q., Sun, Y., Ruehl, C. R., and Setyan, A.: Effect of aqueous-phase processing on aerosol chemistry and size distributions in Fresno, California, during wintertime, Environ. Chem., 9, 221-235, http://dx.doi.org/10.1071/EN11168, 2012.

Gibson, E. R., Hudson, P. K., and Grassian, V. H.: Physicochemical properties of nitrate aerosols: implications for the atmosphere, J. Phys. Chem. A, 110, 11785-11799, 10.1021/jp063821k,

605   2006.

Goodman, A., Underwood, G., and Grassian, V.: A laboratory study of the heterogeneous reaction of nitric acid on calcium carbonate particles, J. Geophys. Res. Atmos., 105, 29053-29064, 2000.

Guo, S., Hu, M., Zamora, M. L., Peng, J., Shang, D., Zheng, J., Du, Z., Wu, Z., Shao, M., Zeng, L.,

610   Molina, M. J., and Zhang, R.: Elucidating severe urban haze formation in China, Proc. Natl. Acad. Sci. U.S.A., 111, 17373-17378, 10.1073/pnas.1419604111, 2014.

Hayes, P. L., Ortega, A. M., Cubison, M. J., Froyd, K. D., Zhao, Y., Cliff, S. S., Hu, W. W., Toohey,

D. W., Flynn, J. H., Lefer, B. L., Grossberg, N., Alvarez, S., Rappenglück, B., Taylor, J. W., Allan, J. D., Holloway, J. S., Gilman, J. B., Kuster, W. C., de Gouw, J. A., Massoli, P., Zhang, X., Liu, J., Weber, R. J., Corrigan, A. L., Russell, L. M., Isaacman, G., Worton, D. R., Kreisberg, N. M., Goldstein, A. H., Thalman, R., Waxman, E. M., Volkamer, R., Lin, Y. H., Surratt, J. D., Kleindienst, T. E., Offenberg, J. H., Dusanter, S., Griffith, S., Stevens, P. S., Brioude, J., Angevine, W. M., and Jimenez, J. L.: Organic aerosol composition and sources in Pasadena, California, during the 2010 CalNex campaign, J. Geophys. Res. Atmos., 118, 9233-9257, 10.1002/jgrd.50530, 2013.

He, H., Wang, Y., Ma, Q., Ma, J., Chu, B., Ji, D., Tang, G., Liu, C., Zhang, H., and Hao, J.: Mineral dust and NOx promote the conversion of SO_2 to sulfate in heavy pollution days, Sci. Rep., 4, 10.1038/srep04172, 2014.

Hu, W., Campuzano-Jost, P., Day, D. A., Croteau, P., Canagaratna, M. R., Jayne, J. T., Worsnop, D. R., and Jimenez, J. L.: Evaluation of the new capture vaporizer for Aerosol Mass Spectrometers (AMS) through laboratory studies of inorganic species, Atmos. Meas. Tech. Discuss., 2016, 1-55, 10.5194/amt-2016-337, 2016.

Hu, W., Campuzano-Jost, P., Day, D. A., Croteau, P., Canagaratna, M. R., Jayne, J. T., Worsnop, D. R., and Jimenez, J. L.: Evaluation of the new capture vaporizer for aerosol mass spectrometers (AMS) through field studies of inorganic species, Aerosol Sci. Technol., 0-0, 10.1080/02786826.2017.1296104, 2017.

Hu, W. W., Hu, M., Yuan, B., Jimenez, J. L., Tang, Q., Peng, J. F., Hu, W., Shao, M., Wang, M., Zeng, L. M., Wu, Y. S., Gong, Z. H., Huang, X. F., and He, L. Y.: Insights on organic aerosol aging and the influence of coal combustion at a regional receptor site of central eastern China, Atmos. Chem. Phys., 13, 10095-10112, 10.5194/acp-13-10095-2013, 2013.

Huang, R. J., Zhang, Y., Bozzetti, C., Ho, K. F., Cao, J. J., Han, Y., Daellenbach, K. R., Slowik, J. G., Platt, S. M., Canonaco, F., Zotter, P., Wolf, R., Pieber, S. M., Bruns, E. A., Crippa, M., Ciarelli, G., Piazzalunga, A., Schwikowski, M., Abbaszade, G., Schnelle-Kreis, J.,

Zimmermann, R., An, Z., Szidat, S., Baltensperger, U., El Haddad, I., and Prevot, A. S.: High secondary aerosol contribution to particulate pollution during haze events in China, Nature, 514, 218-222, 10.1038/nature13774, 2014.

Huang, X. F., He, L. Y., Hu, M., Canagaratna, M. R., Sun, Y., Zhang, Q., Zhu, T., Xue, L., Zeng, L. W., Liu, X. G., Zhang, Y. H., Jayne, J. T., Ng, N. L., and Worsnop, D. R.: Highly time-resolved chemical characterization of atmospheric submicron particles during 2008 Beijing Olympic Games using an Aerodyne High-Resolution Aerosol Mass Spectrometer, Atmos. Chem. Phys., 10, 8933-8945, 10.5194/acp-10-8933-2010, 2010.

Jayne, J. T., Leard, D. C., Zhang, X., Davidovits, P., Smith, K. A., Kolb, C. E., and Worsnop, D. R.: Development of an aerosol mass spectrometer for size and composition analysis of submicron particles, Aerosol Sci. Technol., 33, 49-70, 2000.

Jimenez, J. L., Jayne, J. T., Shi, Q., Kolb, C. E., Worsnop, D. R., Yourshaw, I., Seinfeld, J. H., Flagan, R. C., Zhang, X., Smith, K. A., Morris, J. W., and Davidovits, P.: Ambient aerosol sampling using the Aerodyne Aerosol Mass Spectrometer, J. Geophys. Res. Atmos., 108, 8425, 10.1029/2001JD001213, 2003.

Jimenez, J. L., Canagaratna, M. R., Donahue, N. M., Prevot, A. S. H., Zhang, Q., Kroll, J. H., DeCarlo, P. F., Allan, J. D., Coe, H., Ng, N. L., Aiken, A. C., Docherty, K. S., Ulbrich, I. M., Grieshop, A. P., Robinson, A. L., Duplissy, J., Smith, J. D., Wilson, K. R., Lanz, V. A., Hueglin, C., Sun, Y. L., Tian, J., Laaksonen, A., Raatikainen, T., Rautiainen, J., Vaattovaara, P., Ehn, M., Kulmala, M., Tomlinson, J. M., Collins, D. R., Cubison, M. J., Dunlea, J., Huffman, J. A., Onasch, T. B., Alfarra, M. R., Williams, P. I., Bower, K., Kondo, Y., Schneider, J., Drewnick, F., Borrmann, S., Weimer, S., Demerjian, K., Salcedo, D., Cottrell, L., Griffin, R., Takami, A., Miyoshi, T., Hatakeyama, S., Shimono, A., Sun, J. Y., Zhang, Y. M., Dzepina, K., Kimmel, J. R., Sueper, D., Jayne, J. T., Herndon, S. C., Trimborn, A. M., Williams, L. R., Wood, E. C., Middlebrook, A. M., Kolb, C. E., Baltensperger, U., and Worsnop, D. R.: Evolution of organic aerosols in the atmosphere, Science, 326, 1525-1529, 10.1126/science.1180353, 2009.

665 Lanz, V. A., Prévôt, A. S. H., Alfarra, M. R., Weimer, S., Mohr, C., DeCarlo, P. F., Gianini, M. F. D., Hueglin, C., Schneider, J., Favez, O., D'Anna, B., George, C., and Baltensperger, U.: Characterization of aerosol chemical composition with aerosol mass spectrometry in Central Europe: an overview, Atmos. Chem. Phys., 10, 10453-10471, 10.5194/acp-10-10453-2010, 2010.

670 Li, Y. J., Sun, Y., Zhang, Q., Li, X., Li, M., Zhou, Z., and Chan, C. K.: Real-time chemical characterization of atmospheric particulate matter in China: A review, Atmos. Environ., http://dx.doi.org/10.1016/j.atmosenv.2017.02.027, 2017.

Liu, M., Song, Y., Zhou, T., Xu, Z., Yan, C., Zheng, M., Wu, Z., Hu, M., Wu, Y., and Zhu, T.: Fine Particle pH during Severe Haze Episodes in Northern China, Geophys. Res. Lett., 44, 5213–

675 5221, 10.1002/2017GL073210, 2017.

Liu, P. S. K., Deng, R., Smith, K. A., Williams, L. R., Jayne, J. T., Canagaratna, M. R., Moore, K., Onasch, T. B., Worsnop, D. R., and Deshler, T.: Transmission efficiency of an aerodynamic focusing lens system: Comparison of model calculations and laboratory measurements for the aerodyne Aerosol Mass Spectrometer, Aerosol Sci. Technol., 41, 721-733,

680 10.1080/02786820701422278, 2007.

Middlebrook, A. M., Bahreini, R., Jimenez, J. L., and Canagaratna, M. R.: Evaluation of composition-dependent collection efficiencies for the aerodyne Aerosol Mass Spectrometer using field data, Aerosol Sci. Technol., 46, 258-271, 10.1080/02786826.2011.620041, 2012.

Mohr, C., DeCarlo, P. F., Heringa, M. F., Chirico, R., Slowik, J. G., Richter, R., Reche, C., Alastuey,

685 A., Querol, X., Seco, R., Peñuelas, J., Jiménez, J. L., Crippa, M., Zimmermann, R., Baltensperger, U., and Prévôt, A. S. H.: Identification and quantification of organic aerosol from cooking and other sources in Barcelona using aerosol mass spectrometer data, Atmos. Chem. Phys., 12, 1649-1665, 10.5194/acp-12-1649-2012, 2012.

Ng, N. L., Canagaratna, M. R., Jimenez, J. L., Chhabra, P. S., Seinfeld, J. H., and Worsnop, D. R.:

690 Changes in organic aerosol composition with aging inferred from aerosol mass spectra, Atmos.

Chem. Phys., 11, 6465-6474, 10.5194/acp-11-6465-2011, 2011a.

Ng, N. L., Herndon, S. C., Trimborn, A., Canagaratna, M. R., Croteau, P. L., Onasch, T. B., Sueper, D., Worsnop, D. R., Zhang, Q., Sun, Y. L., and Jayne, J. T.: An Aerosol Chemical Speciation Monitor (Q-ACSM) for routine monitoring of the composition and mass concentrations of ambient aerosol, Aerosol Sci. Technol., 45, 780-794, 10.1080/02786826.2011.560211, 2011b.

Orsini, D. A., Ma, Y., Sullivan, A., Sierau, B., Baumann, K., and Weber, R. J.: Refinements to the particle-into-liquid sampler (PILS) for ground and airborne measurements of water soluble aerosol composition, Atmos. Environ., 37, 1243-1259, http://dx.doi.org/10.1016/S1352-2310(02)01015-4, 2003.

Paatero, P. and Tapper, U.: Positive matrix factorization: A non-negative factor model with optimal utilization of error estimates of data values, Environmetrics, 5, 111-126, 10.1002/env.3170050203, 1994.

Panteliadis, P., Hafkenscheid, T., Cary, B., Diapouli, E., Fischer, A., Favez, O., Quincey, P., Viana, M., Hitzenberger, R., Vecchi, R., Saraga, D., Sciare, J., Jaffrezo, J. L., John, A., Schwarz, J., Giannoni, M., Novak, J., Karanasiou, A., Fermo, P., and Maenhaut, W.: ECOC comparison exercise with identical thermal protocols after temperature offset correction – instrument diagnostics by in-depth evaluation of operational parameters, Atmos. Meas. Tech., 8, 779–792, doi:10.5194/amt-8-779-2015, 2015.

Peck, J., Gonzalez, L. A., Williams, L. R., Xu, W., Croteau, P. L., Timko, M. T., Jayne, J. T., Worsnop, D. R., Miake-Lye, R. C., and Smith, K. A.: Development of an aerosol mass spectrometer lens system for $PM_{2.5}$, Aerosol Sci. Technol., 50, 781-789, 10.1080/02786826.2016.1190444, 2016.

Petit, J. E., Favez, O., Sciare, J., Crenn, V., Sarda-Estève, R., Bonnaire, N., Močnik, G., Dupont, J. C., Haeffelin, M., and Leoz-Garziandia, E.: Two years of near real-time chemical composition of submicron aerosols in the region of Paris using an Aerosol Chemical Speciation Monitor (Q-ACSM) and a multi-wavelength Aethalometer, Atmos. Chem. Phys., 15, 2985-3005, 10.5194/acp-15-2985-2015, 2015.

Petit, J. E., Favez, O., Albinet, A., and Canonaco, F.: A user-friendly tool for comprehensive evaluation of the geographical origins of atmospheric pollution: Wind and trajectory analyses, Environ. Modell. Softw., 88, 183-187, http://dx.doi.org/10.1016/j.envsoft.2016.11.022, 2017.

720

Pieber, S. M., El Haddad, I., Slowik, J. G., Canagaratna, M. R., Jayne, J. T., Platt, S. M., Bozzetti, C., Daellenbach, K. R., Fröhlich, R., Vlachou, A., Klein, F., Dommen, J., Miljevic, B., Jiménez, J. L., Worsnop, D. R., Baltensperger, U., and Prévôt, A. S. H.: Inorganic salt interference on CO_2^+ in aerodyne AMS and Q-ACSM organic aerosol composition studies, Environ. Sci. Technol., 50, 10494-10503, 10.1021/acs.est.6b01035, 2016.

725

Pope, C. A. and Dockery, D. W.: Health effects of fine particulate air pollution: Lines that connect, J. Air Waste Manage Assoc., 56, 709-742, 10.1080/10473289.2006.10464485, 2006.

Rumsey, I. C., Cowen, K. A., Walker, J. T., Kelly, T. J., Hanft, E. A., Mishoe, K., Rogers, C., Proost, R., Beachley, G. M., Lear, G., Frelink, T., and Otjes, R. P.: An assessment of the performance of the Monitor for AeRosols and GAses in ambient air (MARGA): a semi-continuous method

730

for soluble compounds, Atmos. Chem. Phys., 14, 5639-5658, 10.5194/acp-14-5639-2014, 2014.

Sun, J., Zhang, Q., Canagaratna, M. R., Zhang, Y., Ng, N. L., Sun, Y., Jayne, J. T., Zhang, X., Zhang, X., and Worsnop, D. R.: Highly time- and size-resolved characterization of submicron aerosol

735

particles in Beijing using an Aerodyne Aerosol Mass Spectrometer, Atmos. Environ., 44, 131-140, 10.1016/j.atmosenv.2009.03.020, 2010.

Sun, Y., Wang, Z., Dong, H., Yang, T., Li, J., Pan, X., Chen, P., and Jayne, J. T.: Characterization of summer organic and inorganic aerosols in Beijing, China with an Aerosol Chemical Speciation Monitor, Atmos. Environ., 51, 250-259, 10.1016/j.atmosenv.2012.01.013, 2012a.

740 Sun, Y., Wang, Z., Fu, P., Jiang, Q., Yang, T., Li, J., and Ge, X.: The impact of relative humidity on aerosol composition and evolution processes during wintertime in Beijing, China, Atmos. Environ., 77, 927-934, 10.1016/j.atmosenv.2013.06.019, 2013.

Sun, Y., Jiang, Q., Wang, Z., Fu, P., Li, J., Yang, T., and Yin, Y.: Investigation of the sources and

evolution processes of severe haze pollution in Beijing in January 2013, J. Geophys. Res.

745   Atmos., 119, 4380-4398, 10.1002/2014JD021641, 2014.

Sun, Y., Du, W., Fu, P., Wang, Q., Li, J., Ge, X., Zhang, Q., Zhu, C., Ren, L., Xu, W., Zhao, J., Han, T., Worsnop, D. R., and Wang, Z.: Primary and secondary aerosols in Beijing in winter: sources, variations and processes, Atmos. Chem. Phys., 16, 8309-8329, 10.5194/acp-16-8309-2016, 2016.

750   Sun, Y. L., Zhang, Q., Schwab, J. J., Demerjian, K. L., Chen, W. N., Bae, M. S., Hung, H. M., Hogrefe, O., Frank, B., Rattigan, O. V., and Lin, Y. C.: Characterization of the sources and processes of organic and inorganic aerosols in New York city with a high-resolution time-of-flight aerosol mass apectrometer, Atmos. Chem. Phys., 11, 1581-1602, 10.5194/acp-11-1581-2011, 2011.

755   Sun, Y. L., Zhang, Q., Schwab, J. J., Yang, T., Ng, N. L., and Demerjian, K. L.: Factor analysis of combined organic and inorganic aerosol mass spectra from high resolution aerosol mass spectrometer measurements, Atmos. Chem. Phys., 12, 8537-8551, 10.5194/acp-12-8537-2012, 2012b.

Sun, Y. L., Wang, Z. F., Du, W., Zhang, Q., Wang, Q. Q., Fu, P. Q., Pan, X. L., Li, J., Jayne, J., and

760   Worsnop, D. R.: Long-term real-time measurements of aerosol particle composition in Beijing, China: seasonal variations, meteorological effects, and source analysis, Atmos. Chem. Phys., 15, 14549-14591, 10.5194/acpd-15-14549-2015, 2015.

Trebs, I., Meixner, F. X., Slanina, J., Otjes, R., Jongejan, P., and Andreae, M. O.: Real-time measurements of ammonia, acidic trace gases and water-soluble inorganic aerosol species at a

765   rural site in the Amazon Basin, Atmos. Chem. Phys., 4, 967-987, 10.5194/acp-4-967-2004, 2004.

Turpin, B. J. and Huntzicker, J. J.: Identification of secondary organic aerosol episodes and quantitation of primary and secondary organic aerosol concentrations during SCAQS, Atmos. Environ., 29, 3527-3544, http://dx.doi.org/10.1016/1352-2310(94)00276-Q, 1995.

770   Ulbrich, I. M., Canagaratna, M. R., Zhang, Q., Worsnop, D. R., and Jimenez, J. L.: Interpretation of organic components from Positive Matrix Factorization of aerosol mass spectrometric data, Atmos. Chem. Phys., 9, 2891-2918, 10.5194/acp-9-2891-2009, 2009.

Wang, G., Zhang, R., Gomez, M. E., Yang, L., Levy Zamora, M., Hu, M., Lin, Y., Peng, J., Guo, S., Meng, J., Li, J., Cheng, C., Hu, T., Ren, Y., Wang, Y., Gao, J., Cao, J., An, Z., Zhou, W., Li,

775   G., Wang, J., Tian, P., Marrero-Ortiz, W., Secrest, J., Du, Z., Zheng, J., Shang, D., Zeng, L., Shao, M., Wang, W., Huang, Y., Wang, Y., Zhu, Y., Li, Y., Hu, J., Pan, B., Cai, L., Cheng, Y., Ji, Y., Zhang, F., Rosenfeld, D., Liss, P. S., Duce, R. A., Kolb, C. E., and Molina, M. J.: Persistent sulfate formation from London Fog to Chinese haze, Proc. Natl. Acad. Sci. U.S.A., 10.1073/pnas.1616540113, 2016a.

780   Wang, J., Ge, X., Chen, Y., Shen, Y., Zhang, Q., Sun, Y., Xu, J., Ge, S., Yu, H., and Chen, M.: Highly time-resolved urban aerosol characteristics during springtime in Yangtze River Delta, China: insights from soot particle aerosol mass spectrometry, Atmos. Chem. Phys., 16, 9109-9127, 10.5194/acp-16-9109-2016, 2016b.

Wang, Y. H., Liu, Z. R., Zhang, J. K., Hu, B., Ji, D. S., Yu, Y. C., and Wang, Y. S.: Aerosol

785   physicochemical properties and implications for visibility during an intense haze episode during winter in Beijing, Atmos. Chem. Phys., 15, 3205-3215, 10.5194/acp-15-3205-2015, 2015.

Watson, J. G.: Visibility: Science and Regulation, J. Air Waste Manage Assoc., 52, 628-713, 10.1080/10473289.2002.10470813, 2002.

790   Xie, Y., Ding, A., Nie, W., Mao, H., Qi, X., Huang, X., Xu, Z., Kerminen, V.-M., Petäjä, T., Chi, X., Virkkula, A., Boy, M., Xue, L., Guo, J., Sun, J., Yang, X., Kulmala, M., and Fu, C.: Enhanced sulfate formation by nitrogen dioxide: Implications from in situ observations at the SORPES station, J. Geophys. Res. Atmos., 120, 12679-12694, 10.1002/2015JD023607, 2015.

Xu, J., Zhang, Q., Chen, M., Ge, X., Ren, J., and Qin, D.: Chemical composition, sources, and

795   processes of urban aerosols during summertime in northwest China: insights from high-

resolution aerosol mass spectrometry, Atmos. Chem. Phys., 14, 12593-12611, 10.5194/acp-14-12593-2014, 2014.

Xu, J. Z., Zhang, Q., Wang, Z. B., Yu, G. M., Ge, X. L., and Qin, X.: Chemical composition and size distribution of summertime $PM_{2.5}$ at a high altitude remote location in the northeast of the Qinghai–Xizang (Tibet) Plateau: insights into aerosol sources and processing in free troposphere, Atmos. Chem. Phys., 15, 5069-5081, 10.5194/acp-15-5069-2015, 2015.

Xu, W., Croteau, P., Williams, L., Canagaratna, M., Onasch, T., Cross, E., Zhang, X., Robinson, W., Worsnop, D., and Jayne, J.: Laboratory characterization of an aerosol chemical speciation monitor with $PM_{2.5}$ measurement capability, Aerosol Sci. Technol., 51, 69-83, 10.1080/02786826.2016.1241859, 2017a.

Xu, W., Han, T., Du, W., Wang, Q., Chen, C., Zhao, J., Zhang, Y., Li, J., Fu, P., Wang, Z., Worsnop, D. R., and Sun, Y.: Effects of aqueous-phase and photochemical processing on secondary organic aerosol formation and evolution in Beijing, China, Environ. Sci. Technol., 51, 762-770, 10.1021/acs.est.6b04498, 2017b.

Xue, J., Yuan, Z., Griffith, S. M., Yu, X., Lau, A. K. H., and Yu, J. Z.: Sulfate formation enhanced by a cocktail of high NOx, SO_2, particulate matter, and droplet pH during Haze-Fog events in megacities in China: an observation-based modeling investigation, Environ. Sci. Technol. , 50, 7325-7334, 10.1021/acs.est.6b00768, 2016.

Ye, Z., Liu, J., Gu, A., Feng, F., Liu, Y., Bi, C., Xu, J., Li, L., Chen, H., Chen, Y., Dai, L., Zhou, Q., and Ge, X.: Chemical characterization of fine particulate matter in Changzhou, China, and source apportionment with offline aerosol mass spectrometry, Atmos. Chem. Phys., 17, 2573-2592, 10.5194/acp-17-2573-2017, 2017.

Zhang, J. K., Sun, Y., Liu, Z. R., Ji, D. S., Hu, B., Liu, Q., and Wang, Y. S.: Characterization of submicron aerosols during a month of serious pollution in Beijing, 2013, Atmos. Chem. Phys., 14, 2887-2903, 10.5194/acp-14-2887-2014, 2014.

Zhang, Q., Jimenez, J. L., Canagaratna, M. R., Allan, J. D., Coe, H., Ulbrich, I., Alfarra, M. R.,

Takami, A., Middlebrook, A. M., Sun, Y. L., Dzepina, K., Dunlea, E., Docherty, K., DeCarlo, P. F., Salcedo, D., Onasch, T., Jayne, J. T., Miyoshi, T., Shimono, A., Hatakeyama, S., Takegawa, N., Kondo, Y., Schneider, J., Drewnick, F., Borrmann, S., Weimer, S., Demerjian, K., Williams, P., Bower, K., Bahreini, R., Cottrell, L., Griffin, R. J., Rautiainen, J., Sun, J. Y., Zhang, Y. M., and Worsnop, D. R.: Ubiquity and dominance of oxygenated species in organic aerosols in anthropogenically-influenced Northern Hemisphere midlatitudes, Geophys. Res. Lett., 34, 10.1029/2007gl029979, 2007.

Zhang, Q., Jimenez, J. L., Canagaratna, M. R., Ulbrich, I. M., Ng, N. L., Worsnop, D. R., and Sun, Y.: Understanding atmospheric organic aerosols via factor analysis of aerosol mass spectrometry: a review, Anal. Bioanal. Chem., 401, 3045-3067, 10.1007/s00216-011-5355-y, 2011.

Zhang, R., Wang, G., Guo, S., Zamora, M. L., Ying, Q., Lin, Y., Wang, W., Hu, M., and Wang, Y.: Formation of urban fine particulate matter, Chem. Rev., 115, 3803-3855, 10.1021/acs.chemrev.5b00067, 2015a.

Zhang, Y., Tang, L., Yu, H., Wang, Z., Sun, Y., Qin, W., Chen, W., Chen, C., Ding, A., Wu, J., Ge, S., Chen, C., and Zhou, H.-C.: Chemical composition, sources and evolution processes of aerosol at an urban site in Yangtze River Delta, China during wintertime, Atmos. Environ., 123, Part B, 339-349, 2015b.

Zhang, Y., Tang, L., Sun, Y., Favez, O., Canonaco, F., Albinet, A., Couvidat, F., Liu, D., Jayne, J. T., Wang, Z., Croteau, P. L., Canagaratna, M. R., Zhou, H.-C., Prévôt, A. S. H., and Worsnop, D. R.: Limited formation of isoprene epoxydiols-derived secondary organic aerosol under NOx-rich environments in Eastern China, Geophys. Res. Lett., 44, 2035-2043, 10.1002/2016GL072368, 2017.

Zhang, Y. J., Tang, L. L., Wang, Z., Yu, H. X., Sun, Y. L., Liu, D., Qin, W., Canonaco, F., Prévôt, A. S. H., Zhang, H. L., and Zhou, H. C.: Insights into characteristics, sources, and evolution of submicron aerosols during harvest seasons in the Yangtze River delta region, China, Atmos.

Chem. Phys., 15, 1331-1349, 10.5194/acp-15-1331-2015, 2015c.

850
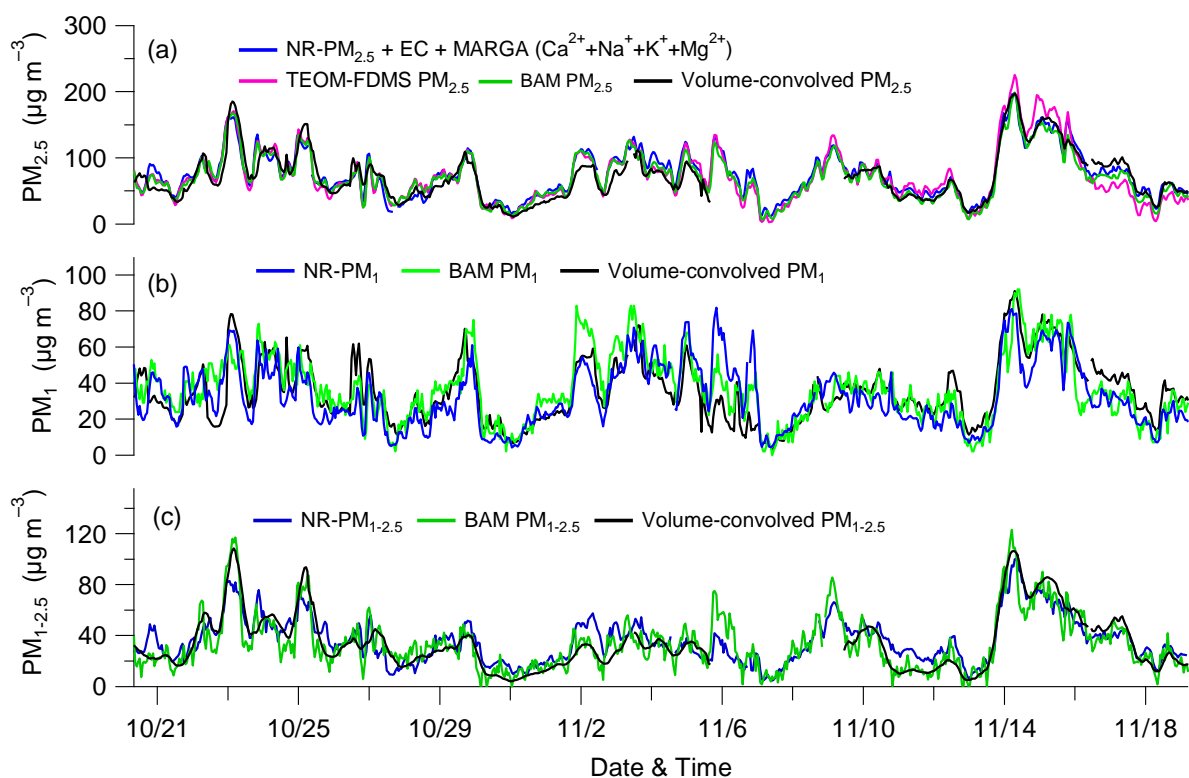
Figure 1. Comparisons between the total particle mass concentrations measured by the PM$_1$ and PM$_{2.5}$ ACSMs, a PM$_{2.5}$ TEOM-FDMS and two MET ONE BAM 1020 (for PM$_1$ and PM$_{2.5}$, respectively), as well as volume-convolved mass calculated from the TDMPS and APS, i.e. PM$_1$ (~13-1000 nm), PM$_{1-2.5}$ (~1000-2500 nm), and PM$_{2.5}$ (~13-2500 nm), and particle density

855   calculated by the ACSM species. Note that NR-PM$_1$ and NR-PM$_{2.5}$ are the mass loadings of the sum of organic, nitrate, sulfate, nitrate, ammonium, and chloride from PM$_1$ and PM$_{2.5}$ ACSM, respectively.
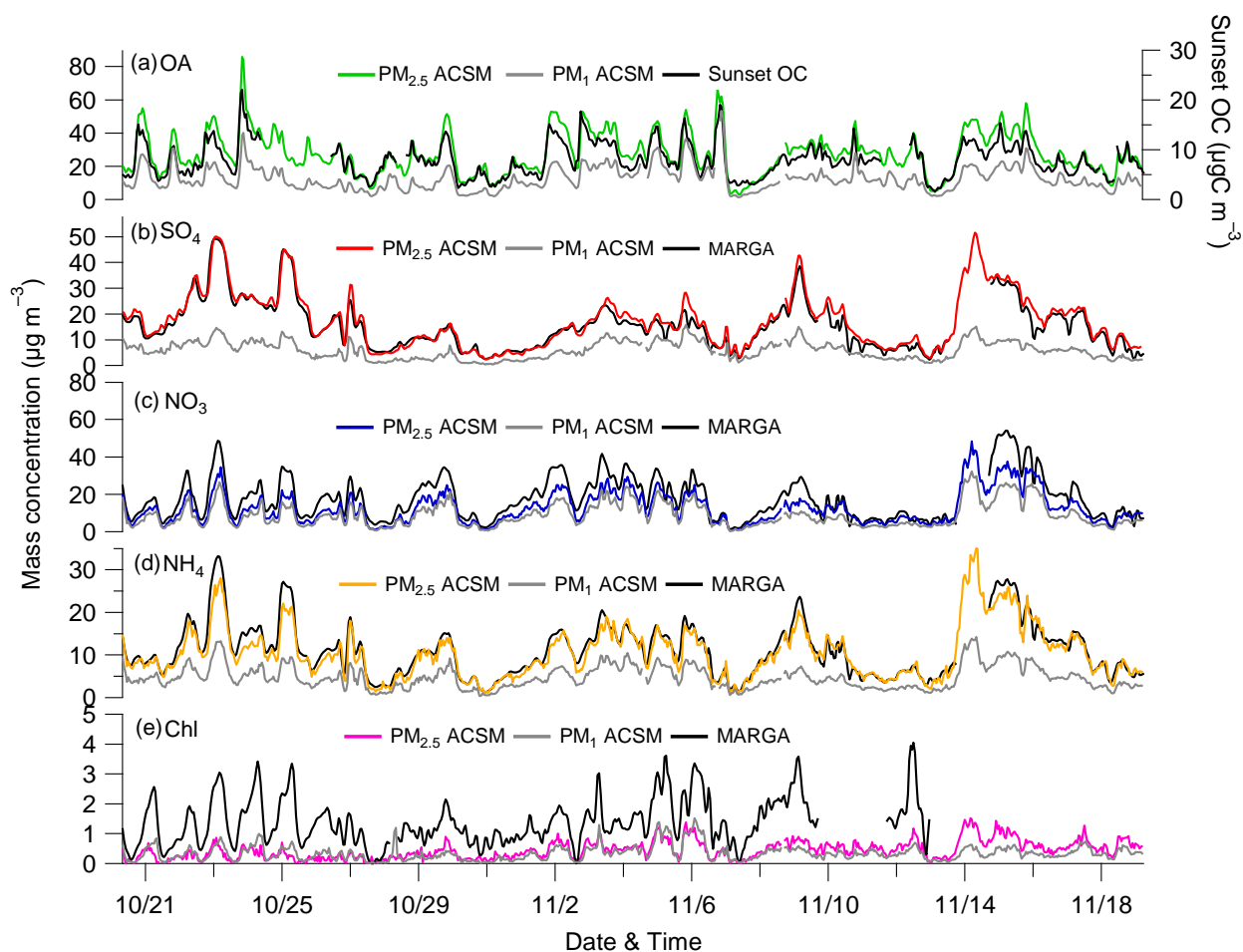
Figure 2. Inter-comparisons between the NR-PM$_{2.5}$ mass concentrations measured by the PM$_1$ and PM$_{2.5}$ ACSMs and the data acquired by collocated instruments: (a) organics vs. PM$_{2.5}$ OC by a Sunset Lab OC/EC Analyzer, and (b–e) sulfate, nitrate, ammonium, and chloride vs. those measured by the PM$_{2.5}$ MARGA.
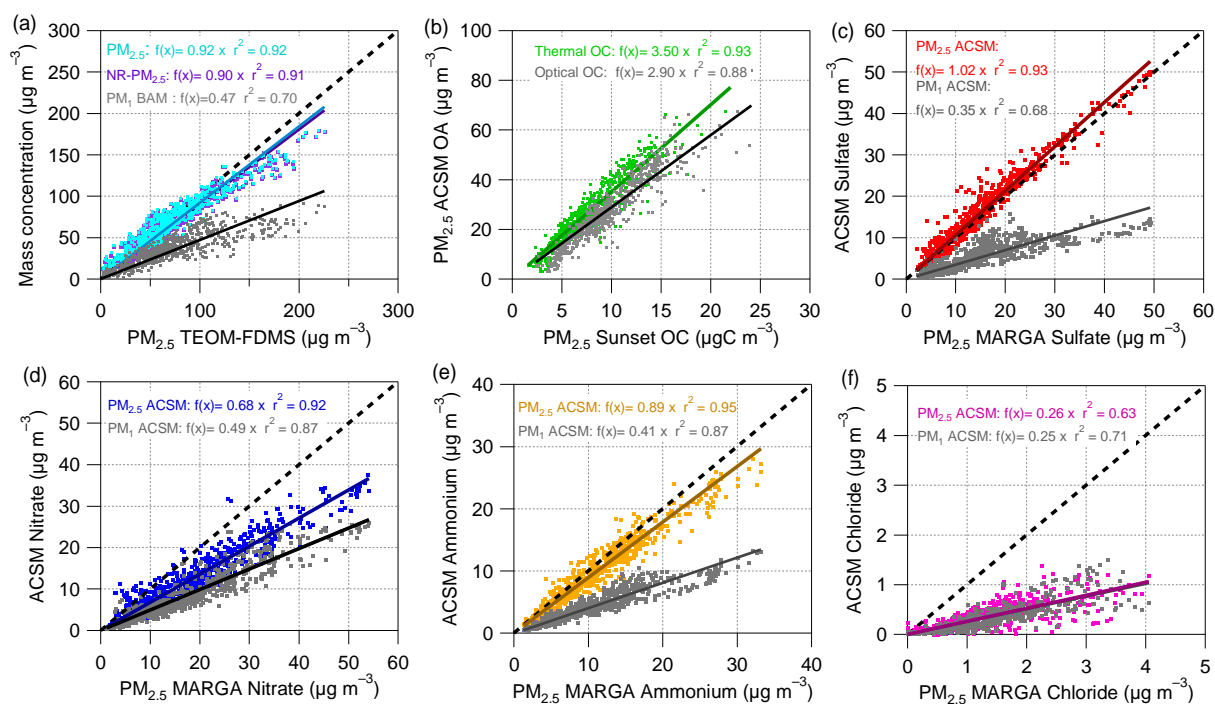
Figure 3. Scatter plots with the linear regression parameters and the 1:1 line (dashed line) shown for the comparisons. Note that the term of "PM$_{2.5}$" in the plot of Fig. 3a means that the summed mass concentration of the PM$_{2.5}$-ACSM species (organics, nitrate, sulfate, ammonium, and chloride), Sunset EC, and MARGA species (K$^+$, Na$^+$, Mg^{2+}, and Ca^{2+}). Also note that the difference observed between "thermal" and "optical" PM$_{2.5}$ OC measurements (Fig. 3b) might be related to poor calibration of the oven temperature probe (e.g., Panteliadis et al., 2015), which couldn't be checked before nor after the campaign.

865

870
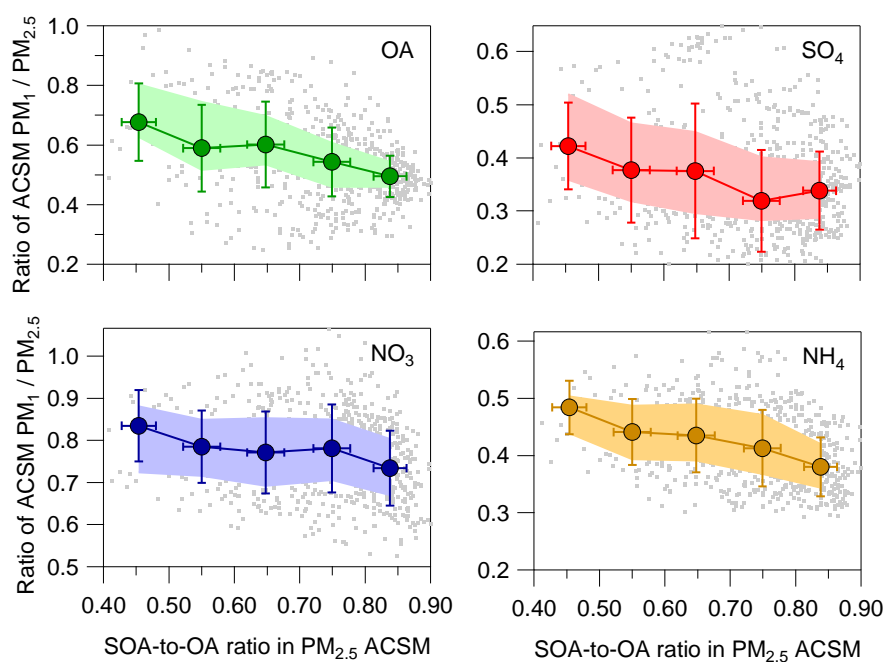
Figure 4. Relationship between the $PM_1/PM_{2.5}$ ratios of aerosol species from the Q-ACSM measurements and the ratio of SOA to OA in $PM_{2.5}$. The error bars refer to the standard deviation. The dots in grey are the raw data points corresponding to Figure 2. The mean (filled circles), 25th and 75th percentiles (lower and upper bands) are also shown.
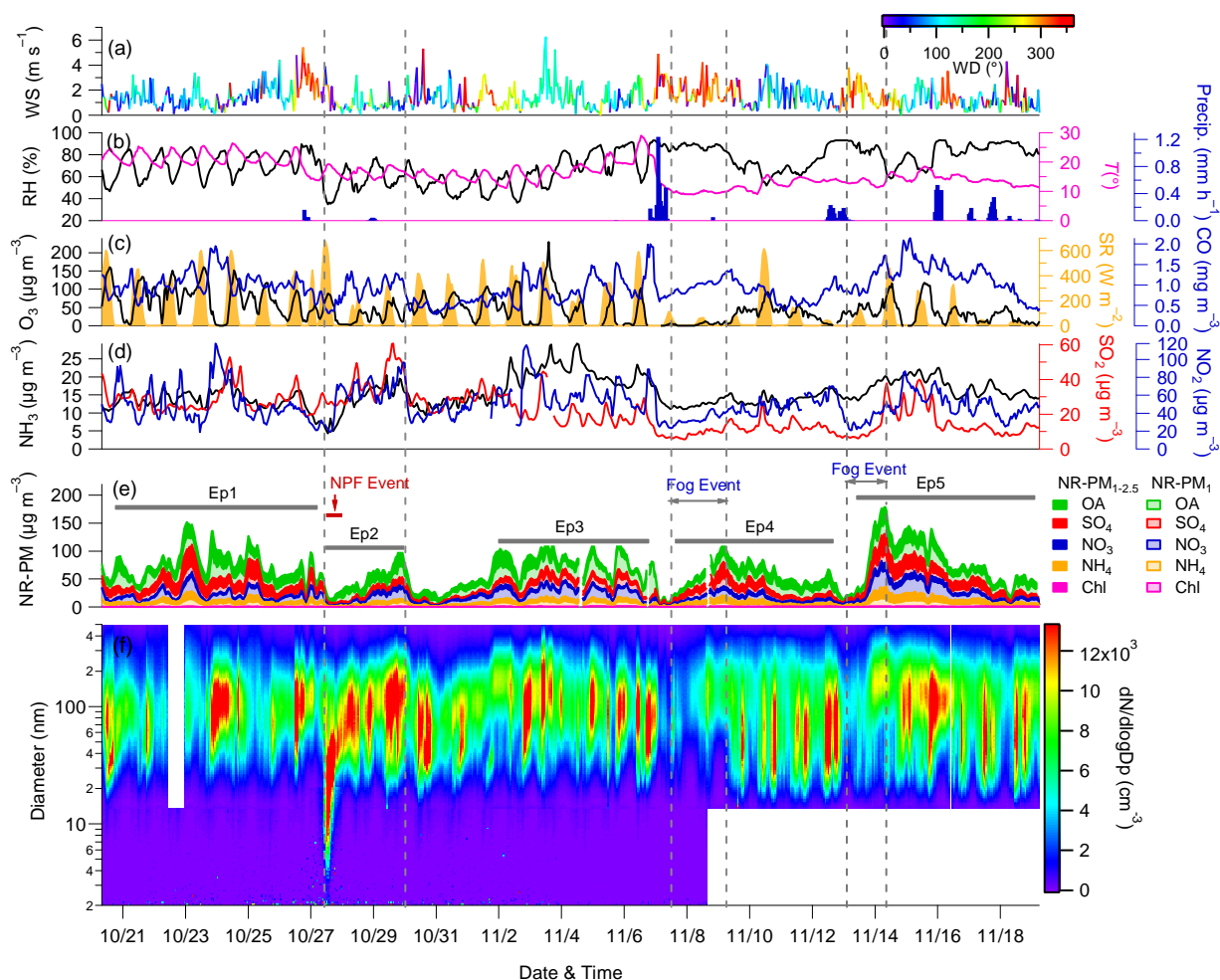
Figure 5. Time series of (a) wind direction (WD) and wind speed (WS); (b) relative humidity (RH), air temperature (T); (c) solar radiation (SR) and O_3; (d) gas-phase NH_3, SO_2 and NO_2; (e) chemical composition of NR-PM (PM_1 and $PM_{1–2.5}$); and (f) size distribution of aerosol particles during the entire study. Note that the white blank areas in (f) are caused by the missing data. In addition, five episodes (Ep1–Ep5) are marked by different pollution events, e.g., persistent haze pollution ($> \sim 5$ days) (Ep1 and Ep3), new particle formation and growth evolution (Ep2), and fog related processes (Ep4 and Ep5).
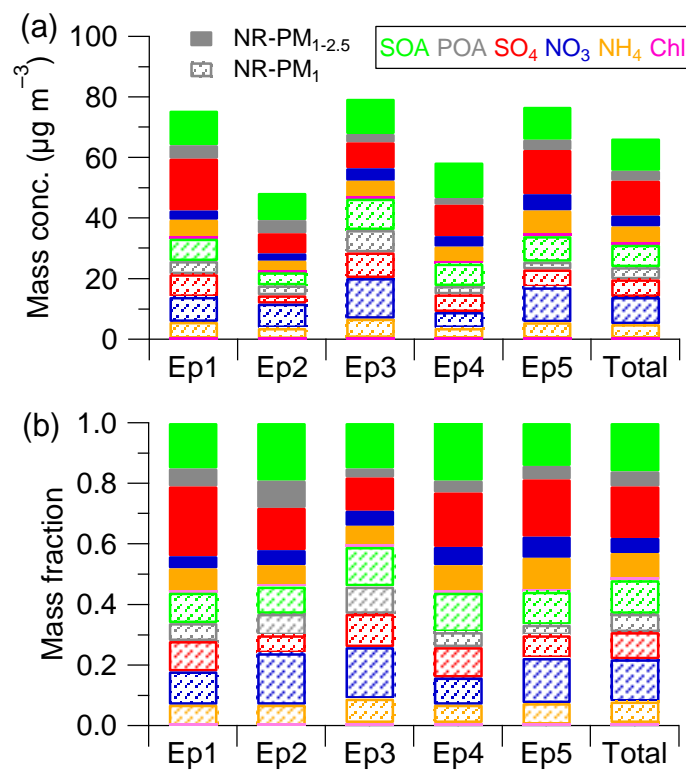
890

Figure 6. Mass concentration (a) and fraction (b) of the NR-PM$_1$ and NR-PM$_{1–2.5}$ chemical components in NR-PM$_{2.5}$ respectively during the different episodes (Ep1–Ep5) marked in Figure 5 and entire study period (Total).

895
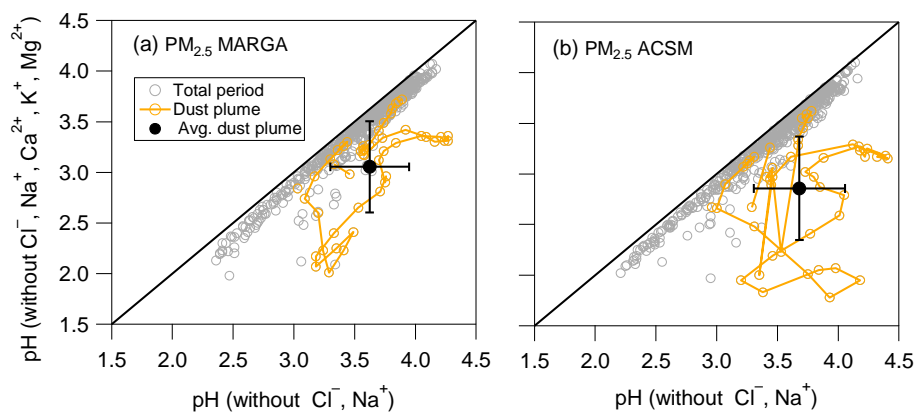
Figure 7. Comparison of predicted fine aerosol pH between with and without Ca^{2+}, K^+, Mg^{2+} as model inputs, for the PM$_{2.5}$-ACSM and PM$_{2.5}$-MARGA, respectively. The dust plume has been marked in Figure S7, during the period of which the PM$_{2.5}$-MARGA pH increased from 3.06 ± 0.45 to 3.62 ± 0.32, and the PM$_{2.5}$-ACSM pH increased from 2.86 ± 0.51 to 3.70 ± 0.37.

900
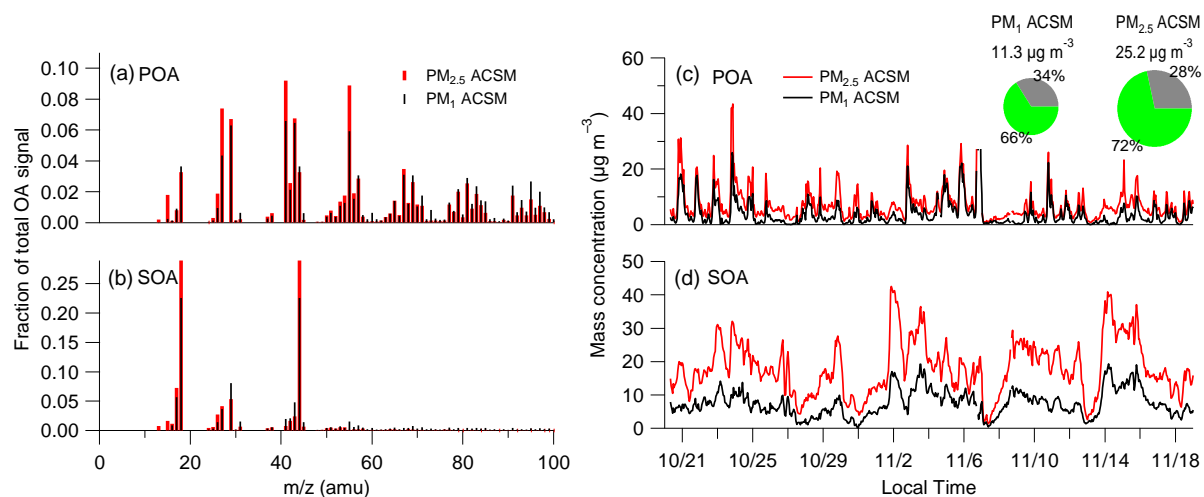
Figure 8. Mass spectra (a and b) and time series (c and d) of POA and SOA for the PM$_1$-ACSM and PM$_{2.5}$-ACSM, respectively. The average mass concentrations and fraction of POA and SOA were added in the sub-plots.

905
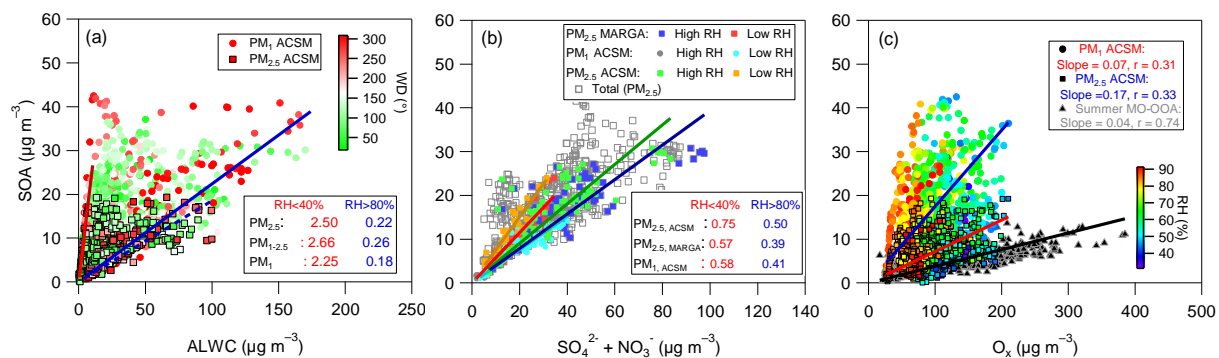
Figure 9. Correlations between (a) NR-PM$_1$ and NR-PM$_{2.5}$ SOA versus ALWC, which is color coded by wind direction (WD); and (b) SOA versus SO$_4^{2-}$ + NO$_3^-$. The regression slopes at high RH (RH > 80 %) and low RH (RH < 40 %) levels and in different size (PM$_1$ and PM$_{2.5}$) are also shown. (c) Relationship between the SOA for NR-PM$_1$ and NR-PM$_{2.5}$ and O$_x$ (= O$_3$ + NO$_2$). The relationship between more oxidized OOA (MO-OOA) and O$_x$ at the same sampling site during summertime (August) 2013 (Zhang et al., 2017) is also shown. Note that the data points during the precipitation periods (Fig. 5b) were removed in these Figs. 9 (a – c).
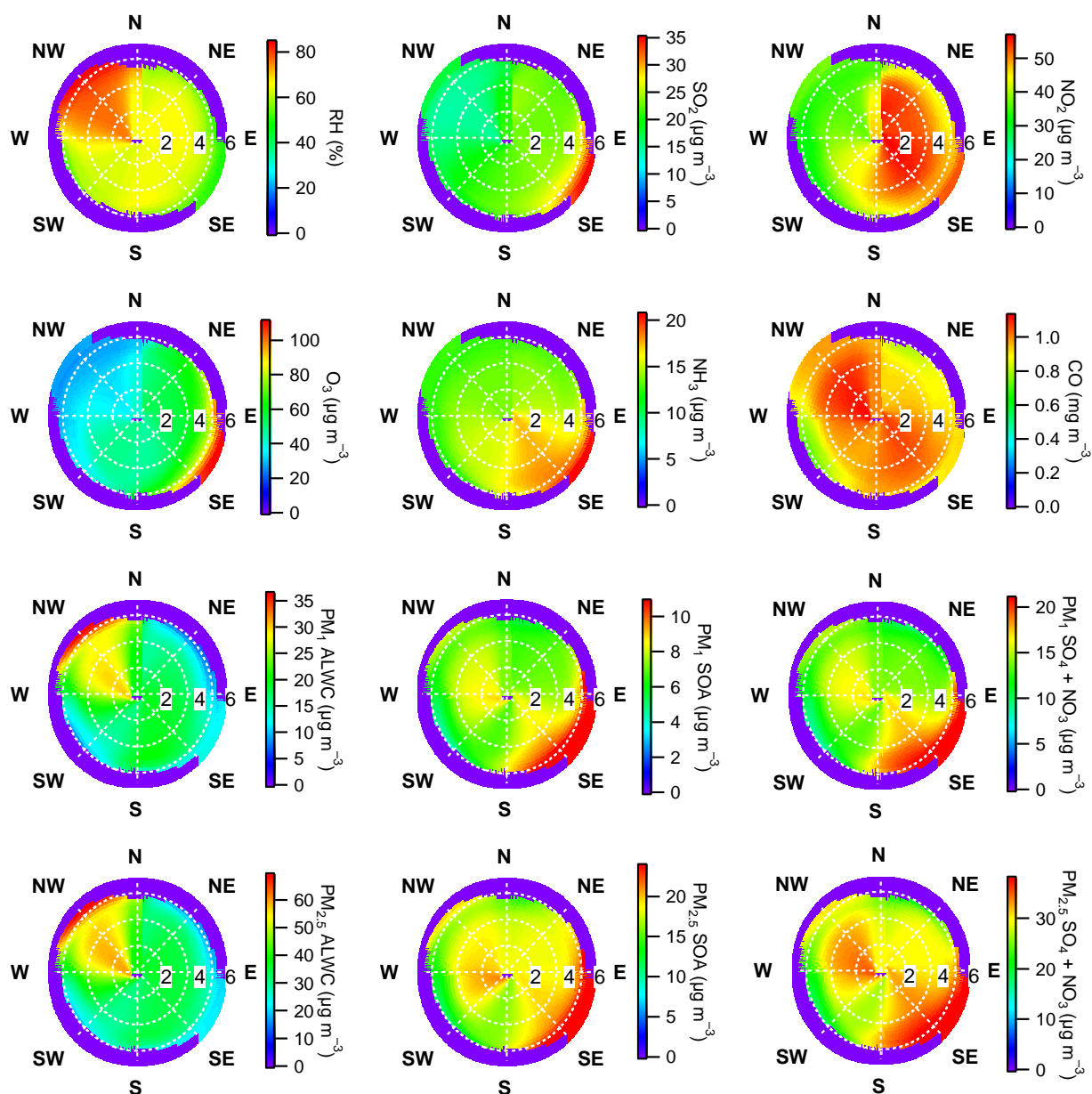
915

Figure 10. Wind analysis on relative humidity (RH), and gas-phase species (SO_2, NO_2, O_3, NH_3, and CO) and PM_1 and $PM_{2.5}$ ALWC, SOA, and [SO_4 + NO_3], respectively. Radius and angle of each plot refers to wind speed (m s^{-1}) and wind direction.

920
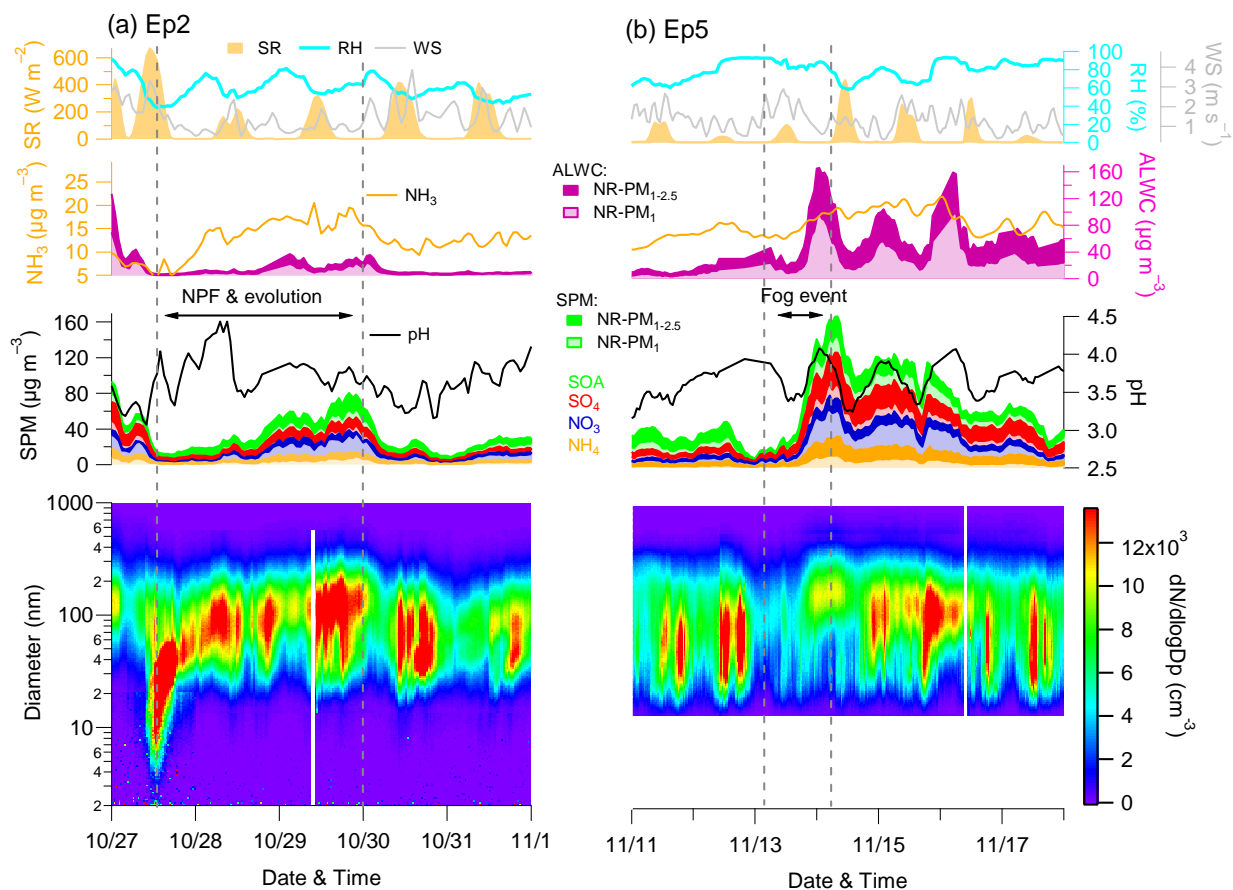
Figure 11. Evolution of meteorological parameters, secondary particulate matter (SPM), and the size distribution during two types of episodes (Ep2 and Ep5).